Chapter 5

Nanotoxicity in Cancer Research: Technical Protocols and Considerations for the Use of 3D Tumour Spheroids

Dania Movia and Adriele Prina-Mello

Additional information is available at the end of the chapter

http://dx.doi.org/10.5772/intechopen.69447

Abstract

The poor clinical translation of oncological nanomedicine products is one of the greatest challenges faced by research today. The use of reductionist *in vitro* models of human cancer and non-predictive animal models is generally considered as one of the main causes of such very low translation rate. The integration of three-dimensional (3D) tumour spheroids in the early stages of the preclinical screening pipeline could significantly facilitate the translation of nanomedicine candidates into clinical practice, by allowing for a more reliable prediction of their efficacy and safety in humans. To lead a successful integration of 3D spheroids, protocols that satisfy issues of ease-of-use, reproducibility and compatibility with conventional and high-throughput assays, without losing the advantages offered by two-dimensional (2D) cell systems, are still needed. To address such need, protocols for the formation and characterisation of scaffold-free 3D tumour spheroids of human adenocarcinoma cells were developed and optimised in this study for their application in nanomedicine safety testing. The protocols reported in this chapter provide the ground on how 3D tumour spheroids could be implemented to design nanomedicine products and speed up experimental cancer research, eliminating those candidates that are likely to be ineffective or unsafe in human at early development stages.

Keywords: 3D tumour spheroids, lung cancer, drug discovery, nanomedicine, safety

1. Introduction

Due to the lack of effective treatment schemes and the high mortality associated with many malignancies, the efforts of the pharmaceutical industry have recently focused on

developing new target-oriented nanomedicine products for improving the cancer patients' survival rate [1].

In parallel to novel targeted anticancer drugs (e.g. imatinib, trastuzumab, crizotinib and vemurafenib) [2], various nanomedicine products [3, 4] have been approved for clinical use in recent times, for more effective and safer cancer treatment. Nevertheless, the attrition rate of more than 90% for new drug candidates entering clinical trials is raising increasing concern [5–7]. One of the major reasons for drugs failure, accounting for around 60% of failed clinical trials, is the lack of efficacy in humans [8–10], albeit the therapeutic effect was robustly demonstrated earlier in preclinical studies. The translation rate of nanomedicine products into real clinical anticancer treatments is also worryingly low [3, 11]. Limitations in the preclinical toolbox currently used in the drug discovery pipeline are believed to be one of the major causes for such growing failures and poor translation [5, 12–14]. For example, doubts as to the relevance of animal models in preclinical studies have been raised: various systematic reviews [15–21] describe in fact the inadequateness of animal research for the efficacy assessments of new drug candidates. Conventional two-dimensional (2D) *in vitro* models are likewise considered as highly reductionist [22], endangering the relevance of the preclinical efficacy data collected [5]. Thus, the integration of new preclinical models in the drug development pipeline is urgently needed.

In order to downtrend the raising failure rates in clinical trials, to increase successful clinical translation with reduced R&D costs and animal experimentation, and ultimately to find new and safe cancer therapies (**Figure 1**), preclinical models must better reflect human *in vivo* conditions. This will assist the clear identification of compounds that have the potential to target specifically and selectively those receptors, markers or cellular behaviours characteristic of malignant cells, allowing for newly identified compounds and nanomedicine products to benefit from enhanced efficacy.

There is overwhelming evidence that *in vitro* three-dimensional (3D) tumour spheroids (i.e. microscale 3D spherical cultures of living cancer cells cultured under non-adherent conditions [23] can provide predictive information on drug efficacy and safety in a smart, cost- and time-effective manner [24]. 3D tumour spheroids can be formed by either self-assembling or by forcing cells to grow as cell clusters starting from single cell suspensions [25]. Conventional methods for spheroid formation include hanging drops, culture of cells on non-adherent surfaces, spinner flask cultures and rotary cell culture systems [26].

It has been demonstrated that 3D tumour spheroids more accurately reflect the responses of human tumours than simple 2D cell cultures [27], in particular with respect to drug sensitivity [28, 29] and nanomedicine efficacy [30]. Some targeted compounds have already proven to be more effective in 3D spheroids than in 2D cultures [31, 32]. In general, however, tumour cells cultured in 3D exhibit significantly increased drug resistance compared to those grown in 2D monolayer cultures. For example, in spheroid models of colorectal cancer [33] and pancreatic cancer [34], a reduction in the responsiveness to antitumour

http://dx.doi.org/10.5772/intechopen.69447

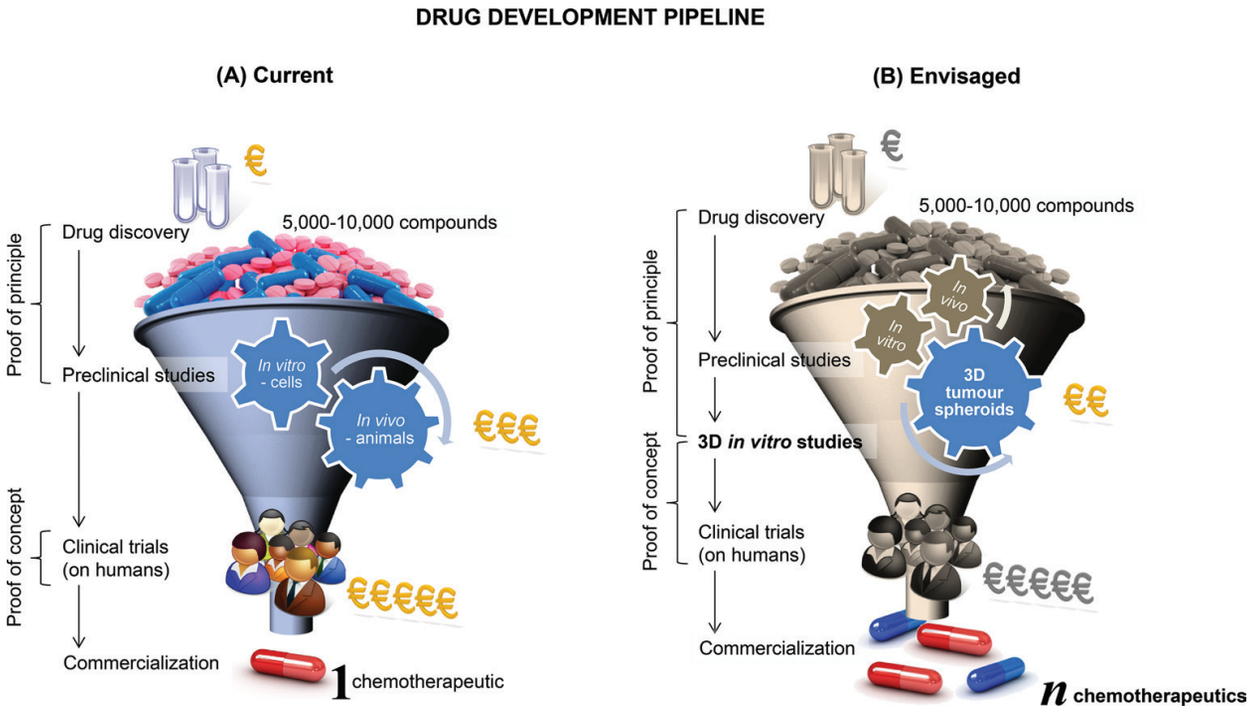

Figure 1. Scheme of the drug development pipeline (A) currently in use and (B) envisaged *via* the implementation of new and more predictive preclinical models. (A) Once active compounds have been identified through the process of drug discovery, preclinical research (*in vitro* studies on cultured cells and *in vivo* studies on animals) are carried out, followed by clinical trials (on humans). Drug development is costly, in particular when carrying out *in vivo* and clinical studies. The current drug development pipeline leads to only one successful market product over 5000–10,000 active compounds identified. (B) Advanced preclinical models capable of predicting drug failures earlier in the 'proof-of-principle' stage, prior to entering costly *in vivo* and clinical studies, will decrease the overall costs of drug development. Studies on 3D tumour spheroids may help significantly, filtering out as early as possible compounds that may not be successful in *in vivo* and clinical studies, thus decreasing the total cost of drug development and increasing the success rate of active compounds in reaching the market as effective chemotherapeutic agents.

agents was observed as a function of multicellular 3D architecture. Multicellular drug resistance is not a new concept and has been studied for the past three decades [35–42]. It is associated with the ability of 3D tumour spheroids from human cancer cell lines to mimic cell dormancy [43, 44]. Cell dormancy originates from the fact that cancer cells in poorly vascularised tumour regions need to adapt to an unfavourable metabolic microenvironment [45], stopping cell cycle progression and becoming dormant. This can confer cancer cells the resistance to drug treatment in humans [46–48]. 3D tumour spheroids can also reproduce cell-cell interactions between cancer cells and/or cancer cells and stroma [49–51]. These interactions strongly influence tumour cells [52] in relation to growth [53], metastasis [53] and response to radio-/chemo-therapy [54]. Various studies have shown in fact that radio- and chemo-resistance of cancer cells is associated with cell-cell adhesion [55]: the term 'cell adhesion-mediated drug resistance' (CAM-DR) has been used to describe this resistance phenomenon [56, 57].

For the purpose of translating oncological nanomedicine products, assessing the ability of the nanocarrier to penetrate into the tumour tissue is essential. 3D tumour spheroids do indeed offer a more predictive *in vitro* model for assessing this aspect [58–65]. Such *in vitro* models have also been extensively used in the last years to evaluate the efficacy [62, 66–72] and safety/toxicity [73–76] of various nanomedicine products with oncological applications, as well as to assess the effect of nanomaterials' physico-chemical properties on their ability to act as nanocarriers of anticancer agents [77–83].

Finally, the use of 3D tumour spheroids considerably limits the ethical issues associated with the use of animal preclinical models, in agreement with the '3Rs (Reduction, Refinement, Replacement) principle' of Russell and Burch in animal research [84].

In light of these considerations, 3D tumour spheroids represent (i) a more predictive and accurate preclinical model and (ii) a key milestone towards a faster and sustainable development of effective nanomedicine products. Consequently, research efforts have recently focused towards adopting 3D tumour spheroids into test platforms, and 3D tumour spheroids has been proposed as 'standard-to-be' for the development and optimisation of new chemotherapeutic agents [85, 86]. From the pharmaceutical industry prospective, it has been also widely accepted that incorporation of 3D tumour spheroids into the drug development pipeline can help selecting the most promising drug candidates prior to clinical trials and to determine future-oriented treatment modalities [14, 87]. What still remains unclear is how to produce such *in vitro* models with a significantly higher degree of equivalence to their *in vivo* counterparts, while making them technically feasible for industrial-scale reliable testing [88]. Indeed, this technological gap has highly hindered the implementation of 3D tumour spheroids as testing platform by the pharmaceutical and nanomedicine industries. Our study aims at addressing this gap by reporting standardised protocols for the formation, characterisation and application of scaffold-free 3D tumour spheroids. Non-small cell lung cancer (NSCLC) was chosen as target cancer type because several therapeutic drugs intended for use in this malignancy have recently failed to show major benefit in clinical trials, despite promising preclinical data [89, 90].

2. Relevance of standardised testing in nanotoxicology

There is overwhelming evidence that *in vitro* 3D tumour spheroids more accurately predict the drug sensitivity of human tumours than conventional 2D cultures. In the market, there are several products available for spheroids preparation; however, for many of them operators are left with the burden to optimise the working protocols to their specific needs. The protocols described herein provide technical solutions for the formation of scaffold-free 3D spheroids and for the characterisation of their architecture and protein marker expression. To support the identification of candidates with clinical potential, protocols are provided for the collection of quantitative data on the efficacy and safety of drug nanocarriers (nanomedicine).

http://dx.doi.org/10.5772/intechopen.69447

No further optimisation is needed, with the additional advantage of their full compatibility with contemporary high-throughput technologies.

3. Experimental details

3.1. Reagents

Reagents used in this study were chosen due to their wide availability worldwide. Please note that these can be purchased from other distributors and manufacturers than those listed here, except if differently specified. TryplE™ solution, rhodamine phalloidin, Hoechst 33342 counterstain, Mouse Anti-Human β-catenin primary IgG, Alexa Fluor 568-conjugated Goat anti-Mouse secondary IgG, FITC-conjugated Mouse Anti-Human Occludin IgG, Alexa Fluor 488-conjugated Monoclonal Mouse Anti-Human Connexin-43 IgG, Live/Dead Cytotoxicity kit for mammalian cells and 0.4% Trypan Blue Solution (all from Invitrogen Ltd) were purchased from Bio-Sciences Ltd (Ireland). Phosphate-buffered saline (PBS) tablets, 37% paraformaldehyde (PFA) solution, glutaraldehyde (GA), bovine serum albumin (BSA), Triton X-100, hexamethyldisilazane (HMDS) and absolute ethanol (EtOH) were obtained from Sigma-Aldrich (Ireland). VECTASHIELD transparent mounting medium was purchased from Vector Laboratories Inc. (CA, USA). Sheep Anti-Human Fibronectin Antigen Affinity-purified Polyclonal primary IgG, NorthernLights™ 557-conjugated Anti-Sheep secondary IgG, Goat Anti-Human Vimentin Antigen Affinity-purified Polyclonal primary IgG, and NorthernLights™ 557-conjugated Anti-Goat secondary IgG were purchased from R&D Systems (Ireland). FITC-conjugated Mouse Anti-Human E-cadherin IgG and BD Cycletest™ Plus DNA Reagent Kit was supplied by BD Biosciences (Oxford, UK). Connexin 43 antibody and E-cadherin (24E10) rabbit mAb used for Western blot experiments were purchased from Cell Signalling Technology (Brennan and Company, Ireland).

3.2. Cell culture

Human alveolar adenocarcinoma cells (A549 cell line) (ATCC® CCL-185™) and human lung fibroblasts (MRC-5 cell line) (ATCC® CCL-171™) were obtained from the American Tissue Culture Collection (LGC standards, Middlesex, UK). A549 and MRC-5 cells were cultured in Ham's F12K medium supplemented with 2nM L-glutamine (Gibco, Invitrogen Ltd, Bio-Sciences Ltd, Ireland), 1% penicillin/streptomycin (Gibco, Invitrogen Ltd, Bio-Sciences Ltd, Ireland) and 10% foetal bovine serum (FBS) (Sigma-Aldrich, Ireland).

Cell culture flasks, 24-well low-cell binding plates (Nunc™) and 96-well ultra-low attachment (ULA) plates (Corning Costar) were purchased from Fisher Scientific (Ireland). Happy Cell™ ASM medium and 96-well low-cell binding plates (Biocroi Ltd) were kindly donated by Biocroi Ltd (Ireland). Happy Cell™ ASM medium is a polymer-based suspension media of low viscosity that enables the 3D culture of cells [91]. 96-well flat-bottom, non-treated plates (BD Falcon™) and 96-well U-bottom, non-treated plates (BD Falcon™) were purchased

from BD Biosciences (Oxford, UK). Four-well Millicell EZ slides were supplied by Millipore (Ireland).

3.3. Equipment

A Zeiss 510 meta laser scanning confocal microscope (LSCM) equipped with a Zeiss LSM 5 software and Zeiss Orion Plus He-ion microscope (both from Carl Zeiss, Germany) were used for imaging the 3D tumour spheroids. A Countess™ cell counter (Invitrogen, UK) was used for trypan blue exclusion assay, while BD Accuri C6 flow cytometer (Becton Dickinson Biosciences, UK) was used for high-throughput assays. The Volocity 3D Image Analysis Software (PerkinElmer Inc., MA, USA) was used for surface rendering of Z-stack images and co-localization studies. Flow cytometry was carried out by means of BD Accuri™ C6 flow cytometer (BD Biosciences, Oxford, UK).

4. Technical protocols and considerations

This study describes the protocols for the formation, characterisation and use of 3D tumour spheroids as *in vitro* models for testing nanomedicine products. These protocols, which are simple, validated and reproducible, can be grouped into three main categories (highlighted in blue boxes in **Figure 2**): (1) protocols for the formation of 3D tumour spheroids, (2) protocols for analytical techniques and (3) protocols for specialised applications.

4.1. Formation of 3D tumour spheroids

One aspect commonly missing in all commercially available products for the formation of scaffold-free 3D tumour spheroids is the description of achievable spheroid size. In addition to this, not all available methodologies produce an abundance of 3D spheroids, and often the *in vitro* models formed have different dimension and shape. The direct consequence is that 3D tumour spheroids are often not comparable among studies, as they are formed of cells in different proliferative and metabolic states, raising serious concerns about the reproducibility of data produced. A recent study has in fact showed that a number of morphology parameters (including volume and shape) affect the response of spheroids to treatment [92]. Such lack of reproducibility is hindering the use of 3D tumour spheroids in preclinical tests.

A protocol was developed in this study allowing for the formation of scaffold-free, non-adherent 3D tumour spheroids of A549 cells with or without the use of a reference commercial product (Happy Cell™ ASM) in combination with various commercially available multi-well plates. Our protocol allowed forming 3D models with well-defined and highly reproducible size in a range between 200 μm and 2 mm. In particular, our 3D tumour spheroids mimicked the size of early stage NSCLC at clinical stages 0–I, where the tumour mass has dimensions below 3 cm.

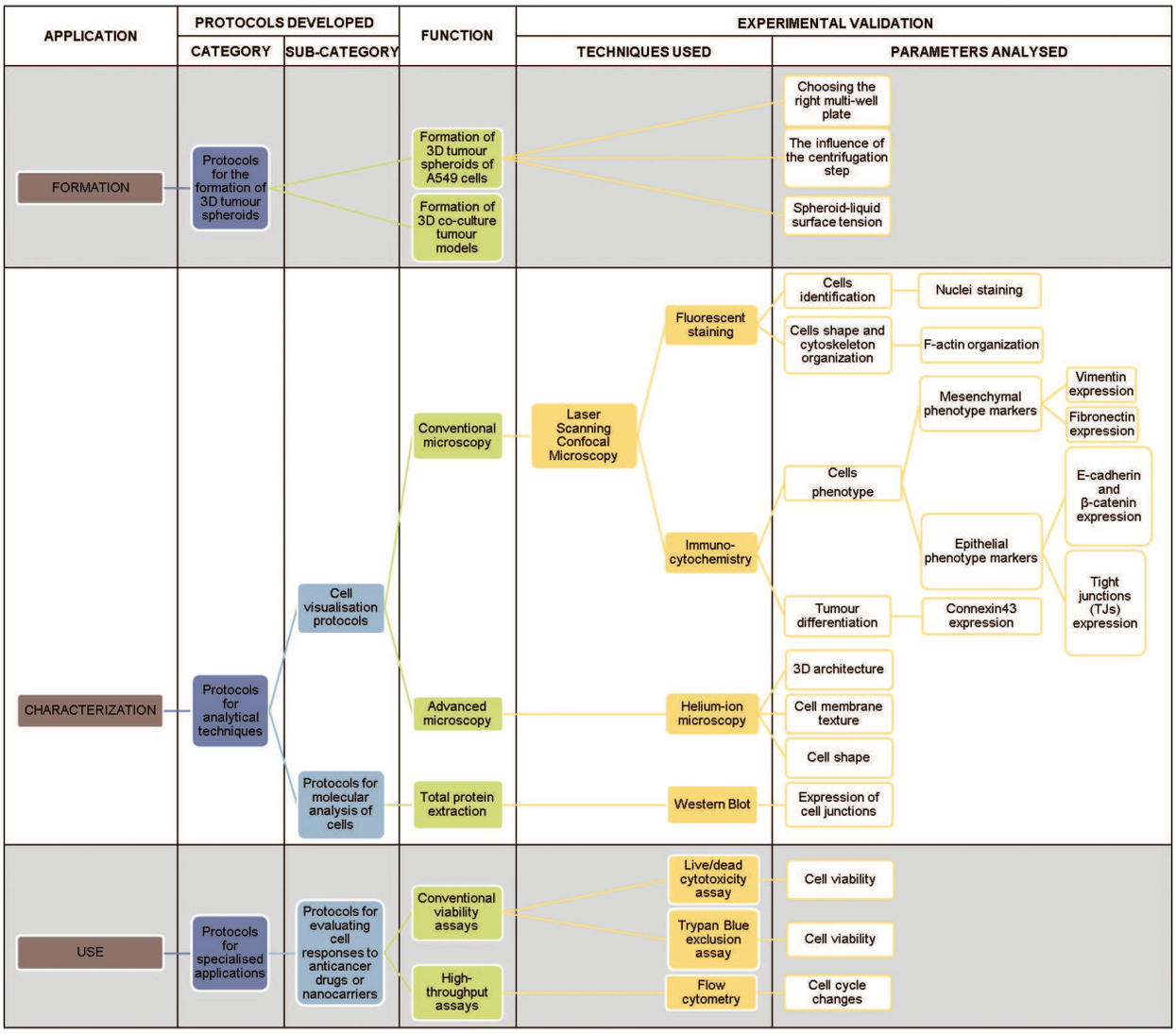

Figure 2. Scheme composing the main application of the protocols developed in this study. Protocols are grouped into three main categories. In some cases, sub-categories can be identified. The protocols developed were validated for their function through experiments analyzing various cellular parameters, by means of standard well-established techniques.

4.1.1. Formation of 3D tumour models of A549 cells

3D tumour spheroids of A549 cells were prepared as described here below.

A. Preparing Happy Cell™ ASM for use:

- Dilute F12K/DMEM Happy Cell™ ASM 2× (commercial product) in Ham's F12K media (supplemented with 2nM L-glutamine, 1% penicillin-streptomycin and 10% foetal bovine serum (FBS)) in 1:9 ratio, thus obtaining Happy Cell™ ASM 1×.

B. Preparing multi-well plates for cell seeding:

- Aliquot Happy Cell™ ASM 1× in a 24-well plate (500 μl/well) or in a 96-well plate (200 μl/well). If using multi-well ultra-low attachment (ULA) plates, the use of Happy Cell™ ASM can be avoided. An equal amount of supplemented media should be aliquoted in its place.
- If preparation of cell suspension is delayed, incubate plates at 37°C, 5% CO_2 until use.

C. Cell seeding:

- Maintain cell line as adherent monolayer cultures in T75 cell culture flasks in Ham's F12K media supplemented with 2 nM L-glutamine, 1% penicillin-streptomycin and 10% FBS. Incubate at 5% CO_2 at 37°C.
- Rinse the cells with phosphate buffered saline (PBS) and add 2 mL of TrypLE™ to detach adherent A549 cells (at 80% confluence) from the culture flask.
- Incubate at 37°C for 3–5 min.
- Neutralise TrypLE™ with 6 mL fresh supplemented Ham's F12K media and centrifuge the cells suspension at 5000 rpm for 4 min.
- Aliquot the cell suspension in 1.5 mL Eppendorf tubes (1 mL cells suspension/tube). For the applications described within this exercise, an initial cell seeding density of 1×10^6 cells/mL in supplemented Ham's F12K media is recommended.
- Centrifugation step: centrifuge the cell suspensions (7200 rpm, 1 min). A cells pellet should form at the bottom of the microtube.
- Carefully aspirate one cells pellet at a time with a sterile, plastic 1000 μL syringe tip.
- Inoculate the cells pellet on the Happy Cell™ ASM 1× (or supplemented media) previously aliquoted in multi-well plates (1 cells pellet/well).
- Incubate for 4 days at 37°C and 5% CO_2. This culture time (spheroid growth phase) is comparable to those reported in the scientific literature [93].

Our experimental data indicated that three main parameters are key in defining the final size of the 3D tumour spheroids formed following our protocol. These are (i) competitive cell adhesion and cell monolayer formation (the stronger is the cell adhesion to the culture substrate, the smaller are the 3D tumour spheroids formed); (ii) initial cell aggregation (the higher cell aggregation is when seeding the cells, the bigger are the 3D tumour spheroids formed) and (iii) the spheroid-liquid surface tension (the lower is the viscosity of the spheroid's surrounding environment, the bigger the spheroids will grow in size). In the next sections, detailed evidence on the importance of such parameters is presented and supported by experimental data.

4.1.1.1. Competitive cell adhesion and cell monolayer formation: selecting the appropriate multi-well plate

Commercially available multi-well plates are available in a variety of formats. In deciding which multi-well plate format to use, the application intended for 3D tumour spheroids should be considered carefully.

The overall tumour response to chemotherapeutic treatments is in fact affected by a multitude of factors, among which is the tumour size. Tumour size is known to strongly affect the diffusion and penetration of molecular and nano-enabled chemotherapeutic treatments decreasing their efficacy [94]. By varying their size, 3D tumour spheroids are thus amenable to therapy-related studies with different emphasis, ranging from studies focusing either on the investigation of the micro-environmental regulation of tumour cell physiology or on the therapeutic efficacy of drugs in authentic pathophysiological milieu conditions. Spheroid size needs therefore to be precisely defined when integrating 3D cell models in drug-testing strategies.

Several commercially available multi-well cell culture plates compatible with high-throughput assays have been tested within this study. In order to perform a comparative assessment of the most suitable multi-well plates for spheroid formation, identical spheroid preparation reagents were used in all relevant experiments. Thus, 3D tumour spheroids were always formed in Happy Cell™ ASM, in combination with various commercially available multi-well plates. The growth of 3D tumour spheroids was monitored by light microscopy for all the tested multi-well plate formats. **Table 1** reports the size distributions of the spheroids obtained in the various plate formats investigated, whereas representative light microscopy images of the 3D tumour spheroids formed are shown in **Figure 3**. Light microscopy imaging showed that 3D tumour spheroids formed in 24-well low-cell binding plates and ULA plates were bigger and more compact, and therefore, more mechanically robust.

4.1.1.2. Initial cell aggregation: the influence of centrifugation on the size of 3D tumour spheroids

Next important feature to consider is how cell aggregation during seeding influences the final size of the 3D tumour spheroids formed. A parallel set of experiments, where cells were seeded avoiding any centrifugation prior to plating, demonstrated the strong influence of this step in defining the final size of the spheroids, except when using 96-well low-cell binding plate. The main outcomes of our experiments (in terms of tumour size) are summarised in **Table 2**. Our results demonstrated that, for obtaining spheroids of size above 1 mm after 4 days in culture, the centrifugation step described in the protocol was necessary.

4.1.1.3. Spheroid-liquid surface tension

As stated above, the viscosity of the spheroid's surrounding environment influences the final size of the *in vitro* model. Our experimental data showed that the dilution factor of Happy Cell™ ASM in supplemented cell culture media contributed to defining the final size of the 3D tumour spheroids formed (**Table 3**). In detail, increasing the viscosity of the surrounding

Multi-well plate format				Spheroid size (mm)	Notes
Number of wells	**Well shape**	**Well surface material**	**Supplier**		
4	Flat-bottom	Glass	Millipore	Not formed	• High cell adhesion • Not suitable
24	Flat-bottom	Low-cell binding polystyrene	Nunc™	1.5 ± 0.5	• Optimal substrate • No cell adhesion • Mechanically robust spheroids
96	Flat-bottom	Low-cell binding polystyrene	Biocroi Ltd	0.18 ± 0.11	• Partial cell adhesion
		ULA polystyrene	Corning Costar	0.85 ± 0.55	• Optimal substrate • No cell adhesion • Mechanically robust spheroids • 3D spheroids size without Happy Cell™ ASM: 0.3–1.3 mm
		Non-treated polystyrene	BD Falcon™	0.4 ± 0.1	• Partial cell adhesion
	U-bottom	Non-treated polystyrene	BD Falcon™	0.35 ± 0.25	

Tumour spheroids were grown in Happy Cell™ ASM at a 1:9 (Happy Cell™ ASM: supplemented media) dilution ratio. With exemption of 96-well plates from Biocroi Ltd., all multi-well plate formats tested are gold-standard cell culture substrates available from conventional suppliers. Cell culture plates provided by Biocroi Ltd. are included for comparison, as a recommended substrate for spheroids growth in Happy Cell™ ASM.

Table 1. Multi-well plate formats tested and main experimental outcomes in respect to the size of 3D tumour spheroids formed.

environment by reducing the dilution of Happy Cell™ ASM to a 1:1 (Happy Cell™ ASM: supplemented media) ratio caused a reduction in tumour spheroids size, except in ULA plates. Thus, our results suggested that, for obtaining spheroids of size above 1 mm, a 1:9 (Happy Cell™ ASM: supplemented media) ratio or the use of ULA multi-well plates (in combination or without Happy Cell™ ASM) is recommended.

4.1.2. Formation of 3D co-culture tumour models

3D co-culture tumour models including heterotypic cellular components (also referred to as multicellular spheroid (MCS) models or multicellular 3D tumour spheroids) play a critical role in recreating the tumour microenvironment *in vitro*. The tumour microenvironment plays a critical role in cancer cell differentiation, and greatly impacts therapeutic efficiency of chemotherapeutic drugs. Co-culture 3D tumour models represent therefore one of the most promising *in vitro* systems for predictive testing of compound efficacy in oncology [94]. Thus, in this study, we developed protocols allowing the formation of a 3D co-culture tumour model that aims to analyse the interplay of NSCLC cells and the healthy surrounding connective tissue. In detail, our model comprised 3D tumour spheroids of lung cancer epithelial

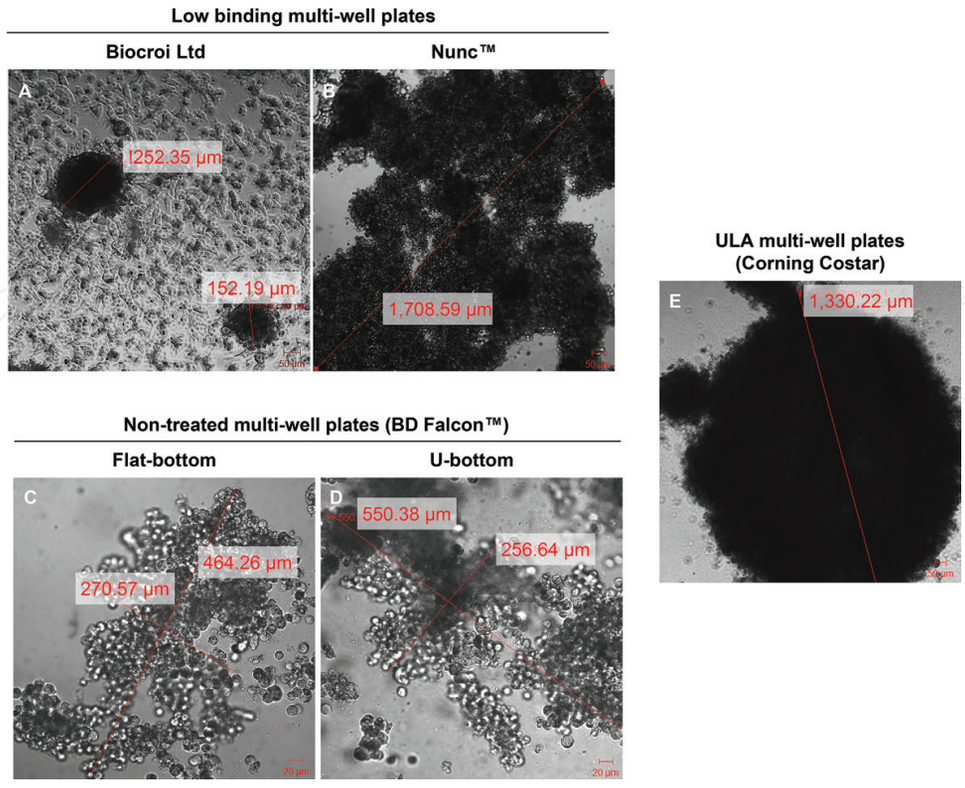

Figure 3. Comparison of 3D tumour spheroids size formed in various multi-well plate formats: (A) 96-well low-cell binding plate; (B) 24-well low-cell binding plate; (C–D) 96-well non-treated plate with (C) flat-bottom or (D) U-bottom wells; and (E) 96-well ULA plate. Tumour spheroids were grown in Happy Cell™ ASM at a 1:9 (Happy Cell™ ASM: supplemented media) dilution ratio.

Multi-well plate format				Spheroid size (mm)	Consequences of lack of centrifugation step
Number of wells	Well shape	Well surface material	Supplier		
4	Flat-bottom	Glass	Millipore	Not formed	• None
24	Flat-bottom	Low-cell binding polystyrene	Nunc™	0.75 ± 0.5	• Decreased spheroids size
96	Flat-bottom	Low-cell binding polystyrene	Biocroi Ltd	0.14 ± 0.06	• No significant changes in spheroids size
		ULA polystyrene	Corning Costar	0.23 ± 0.16	• Decreased spheroids size
		Non-treated polystyrene	BD Falcon™	0.15 ± 0.05	• Decreased spheroids size
	U-bottom	Non-treated polystyrene		0.08 ± 0.02	

Spheroids were grown in Happy Cell™ ASM at a 1:9 (Happy Cell™ ASM: supplemented media) dilution ratio. Conclusions on the consequences associated to the lack of the centrifugation step on the spheroids size are drawn based on the comparison to the spheroid sizes values reported in **Table 1**.

Table 2. Influence of centrifugation step on the final size of the 3D tumour spheroids formed in the various multi-well culture plates tested.

Multi-well plate format				Spheroid size (mm)	Influence of increased viscosity of environment
Number of wells	Well shape	Well surface material	Supplier		
4	Flat-bottom	Glass	Millipore	Not formed	• None
24	Flat-bottom	Low-cell binding polystyrene	Nunc™	1.05 ± 0.15	• Decreased spheroids size
96	Flat-bottom	Low-cell binding polystyrene	Biocroi Ltd	0.15 ± 0.05	• No significant changes in spheroids size
		ULA polystyrene	Corning Costar	1.25 ± 0.75	• Decreased spheroids size
		Non-treated polystyrene	BD Falcon™	0.15 ± 0.05	• Decreased spheroids size
	U-bottom	Non-treated polystyrene		0.2 ± 0.1	

The experimental outcomes (in terms of tumour size) are here reported for spheroids grown in Happy Cell™ ASM at a 1:1 (Happy Cell™ ASM: supplemented media) dilution ratio. The influence of the increased viscosity of the environment on the spheroids size are evaluated based on the comparison to the spheroid sizes values reported in **Table 1**.

Table 3. Influence of the viscosity of the surrounding environment on the final size of the 3D tumour spheroids formed.

(A549) cells cultured on a 2D monolayer of healthy stromal fibroblasts (MRC-5 cells). 3D co-culture tumour models were prepared as described below.

A. Formation of a fibroblast monolayer:

- Maintain MRC-5 cell line as adherent monolayer culture in T75 cell culture flasks in Eagle's Minimum Essential Medium (EMEM) media supplemented with 1% penicillin-streptomycin and 10% FBS, at 5% CO_2 at 37°C.
- Rinse the cells with PBS and add 2 mL of TrypLE™ to detach adherent MRC-5 cells (at 80% confluence) from the culture flask.
- Incubate at 37°C for 3–5 min.
- Neutralise TrypLE™ with 6 mL fresh supplemented EMEM media and centrifuge the cells suspension at 5000 rpm for 4 min.
- Using cell seeding density of 1×10^6 cells/mL in supplemented EMEM media, plate the cells in four-well chambered Millicell EZ slides (final volume: 500 μL/well).
- Incubate for 2/3 days at 37°C and 5% CO_2, until cell monolayer confluence is achieved.

B. Seeding of 3D tumour spheroids:

- With a sterile, plastic 1000 μL syringe tip, carefully aspirate the 3D tumours spheroids previously grown from A549 cells for 4 days with or without Happy Cell™ ASM 1×.

- Inoculate the 3D tumour spheroids on the fibroblast monolayers. It is recommend to use a mixture of supplemented Ham's F12K and EMEM media (ratio 1:1) as culture media for the co-culture 3D tumour models.
- Incubate for 24 h at 37°C and 5% CO_2 to allow the formation of cell-cell adhesions.

Figure 4 shows representative laser scanning confocal microscopy (LSCM) images of the fully formed 3D co-culture tumour models. For specific LSCM staining and imaging protocols please refer to the appropriate sections of this manuscript.

4.2. Protocol for analytical techniques

A wide variety of techniques can be used to study 3D tumour spheroids characteristics. A comprehensive description of such techniques can be found in recently published reviews [26, 95]. The protocols that we describe within this section provide practical guidelines for the application of some of these techniques, allowing for the analytical characterisation of 3D tumour spheroids and 3D co-culture tumour models. These protocols were optimised on 3D tumour spheroids grown in 96-well ULA plates (with or without Happy Cell™ ASM), as these proven to be the most mechanically robust cultures formed. Robustness of 3D tumour spheroids was assessed as for their capability to maintain their shape and size under mechanical stress (e.g. agitation or transfer with a pipette). Conventional two-dimensional (2D) cell monolayers (grown onto glass substrates according to cell supplier guidelines) were used as controls during the validation of our protocols for scaffold-free 3D spheroids.

4.2.1. Cellular imaging

A complete characterisation of the spheroid architecture and protein markers expression in the 3D tumour models used in preclinical studies is crucial for extrapolating and interpreting

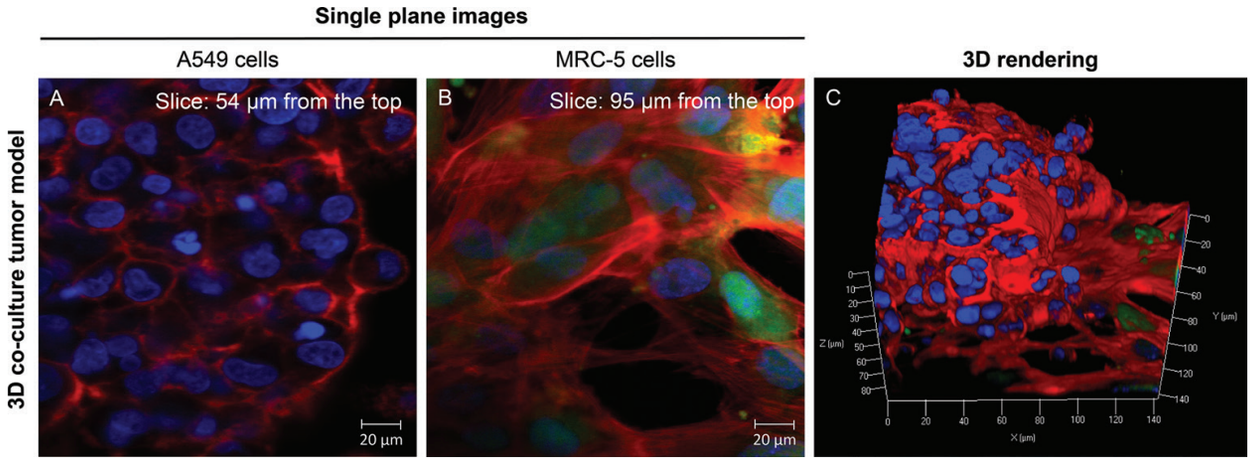

Figure 4. Representative LSCM images of a 3D co-culture tumour model stained for F-actin (rhodamine phalloidin; 1:40 dilution; in red) and nuclei (Hoechst; 1:400 dilution; in blue). MRC-5 cells were also stained with 20 µM Cell Tracker Green CMFDA (in green) for 45 min (37°C and 5% CO_2) prior to seeding the 3D spheroids, to allow their easy identification in the co-culture model. Images were collected in (A–B) single-plane or (C) Z-stack mode with an oil-immersion 63× objective lens. (C) 3D rendering of Z-stack images obtained with the 3D function of Zeiss ZEN software (Carl Zeiss, Germany) (114 sections, total height: 102 µm). (A–C) Scale bars: 10 µm.

valuable data on the efficacy of the molecular or nano-enabled chemotherapeutic agent under investigation. Because scaffold-free 3D tumour spheroids are grown in liquid media and do not adhere to a substrate, such cell models are difficult to image due to the Brownian motion in the culture plates. Thus, the first challenge in imaging scaffold-free tumour spheroids is to stabilise the 3D cell structures, without disrupting their architecture and markers expression, to allow high-quality images to be captured and analysed.

In this study, protocols are described for monitoring and analysing fixed, physically intact spheroid cultures. By applying these protocols it is possible to implement a suite of conventional and advanced imaging technologies, such as LSCM and He-ion microscopy (HIM) to characterise: (i) cells' shape and organisation of their cytoskeleton; (ii) phenotype of the cells forming the 3D tumour spheroids and (iii) the degree of tumour differentiation.

Essential steps needed for preparing 3D tumour spheroids for conventional or advanced imaging analysis are described below.

A. Harvesting:

- At the chosen time point, harvest cells by gentle aspiration of 100 μL/well media. This operation cannot be performed with vacuum pipettes, to avoid accidental aspiration of the 3D tumour spheroids formed.

B. Fixation:

- Add 200 μL/well of fixative and incubate at room temperature.
- Special considerations: fixation of 3D tumour spheroids can be achieved by a chemical approach. Fixation is usually the first stage in a multistep process to prepare a sample for microscopy or other analysis. It is important, when selecting a fixative to have clearly set in mind the final purpose of the analysis, which must be considered and matched by the requirements for the analytical technique. Some fixatives are suitable for general structure analysis, others for immunocytochemistry. Survival of tissue antigens for immunochemical staining depends on the type and concentration of fixative, on fixation time and on the size of the tissue specimen to be fixed. In relation to the suite of conventional and advanced imaging technologies discussed in this study, it is recommended the use of 4% paraformaldehyde (PFA) as fixative for conventional imaging techniques (e.g. LSCM), with an incubation time of 10 min at room temperature. If immunocytochemistry is performed, the selection of the fixative solution should be in accordance with the manufacturer's instructions for the antibodies used. Finally, for advanced imaging analysis (e.g. HIM), immersion in 2.5% glutaraldehyde (GA) for 30 min at room temperature (25°C) is recommended. Incubation overnight at 4°C is also suitable. Avoid longer incubation time, as formaldehyde-derived products can cause cells shrinkage overtime.
- Gently aspirate 200 μL/well.

C. Washing:

- Wash with 200 μL/well PBS by gently adding and then removing the solution to/from the wells.
- Agitation or shacking is to be avoided during this phase to not shear the 3D spheroids from the bottom of the well.

D. Mounting:

- Gently aspirate the 3D tumour spheroids with a 1000 μL tip and transfer them on microscope glass slides.
- Mount the glass slide in transparent mounting medium prior to LSCM analysis—when covering with a glass coverslip, take care not to create air bubbles, then seal with nail varnish or tape. If using nail varnish, leave to dry for at least 30 min at room temperature in the dark before imaging.

E. Storage:

- The stability of the 3D spheroids has been tested at regular intervals: fixed spheroids can be stored in sterile PBS at 4°C up to 1 month.
- Glass slides can be stored in the dark at 4°C up to few months.

4.2.1.1. Conventional microscopy

When viewing an unstained 3D tumour spheroid under brightfield illumination, the combined density and thickness of the 3D culture prevents the clear visualisation of individual cells (as seen in **Figure 3E**). However, fluorescent staining and immunocytochemistry coupled with LSCM can be successfully used to image 3D tumour spheroids at the individual cell level. LSCM relies in fact on the combination of point illumination and a pinhole to eliminate most of the out-of-focus light signal and allows for reconstruction of 3D volumes, making it ideal to image thick samples, such as 3D tumour spheroids.

Here we describe the protocols for the visualisation of various cell markers within 3D tumour spheroids by fluorescent staining or immunocytochemistry. For best results we recommend to acquire Z-stack images by LSCM with intervals in the range between 0.8 and 1.2 μm. Note that spheroids thickness might in some cases exceed the Z-stack capacity of some models of confocal microscopes. Please also note that successful LSCM imaging requires the careful optimization of microscope set-ups. Specific filters, detectors and pinhole size for imaging the specimens might need to be optimised according to the specifications of the microscope and fluorescent dyes used. Long-term exposure of dyes to fluorescent light can lead to photobleaching, so ensuring that shutters closed in between image acquisitions can reduce this problem.

3D tumour spheroids of A549 cells can be stained with fluorescent probes or by immunocytochemistry as described below.

A. Fluorescent staining of fixed 3D tumour spheroids:

- Add staining solution (100 μL/well) to the specimens.
- Incubated for 4 h at room temperature in the dark.
- Wash with 200 μL/well PBS by gently adding and then removing the solution to/from the wells. Repeat the washing step twice.

B. Immunocytochemistry of fixed 3D tumour spheroids

- If a cell permeabilization step is needed, incubate overnight at 4°C with 0.1% Triton X-100 (200 μL/well). The long incubation time is needed to allow the solution to perfuse into the inner core of the 3D tumour spheroids. Note that if using methanol/acetone fixation, no permeabilization step is required.
- Wash with 200 μL/well PBS by gently adding, and then removing the solution to/from the wells.
- Add 200 μL/well blocking buffer (1% BSA) and incubate overnight at 4°C, for avoiding the antibody unspecific binding. It is recommended that for each antibody used, the original manufacturers' instructions regarding blocking reagents must be followed.
- Remove the blocking buffer by gently aspirating 200 μL/well and wash with PBS as previously described (washing step).
- Add the primary antibody (100 μL/well) previously prepared in 0.1% Triton X-100 solution.
- Incubate for 4 h at room temperature. If the antibody is already conjugated to a fluorophore, protect from light.
- Repeat the washing step twice.
- If an unconjugated primary antibody was used, add the secondary (labelled) antibody (100 μL/well) and incubate for 4 h at room temperature in the dark.
- Repeat the washing step twice.

4.2.1.1.1. Experimental validation: cell shape and cell cytoskeleton organisation—F-actin staining

Our protocol for fluorescent staining proved to be useful in quantifying the effect of the surrounding environment when culturing cells in 3D. Similarly to signalling molecules, the mechanical stimuli applied by the surrounding environment to cells induce subcellular and cellular events, such as cytoskeleton remodelling and cell shape changes [96, 97]. 3D tumour spheroids were formed without Happy Cell™ ASM in 96-well ULA plates, stained for F-actin (which is one of the main components of cells' cytoskeleton) and analysed by LSCM. Representative LSCM images of 3D tumour spheroids are shown in **Figure 5**. A549

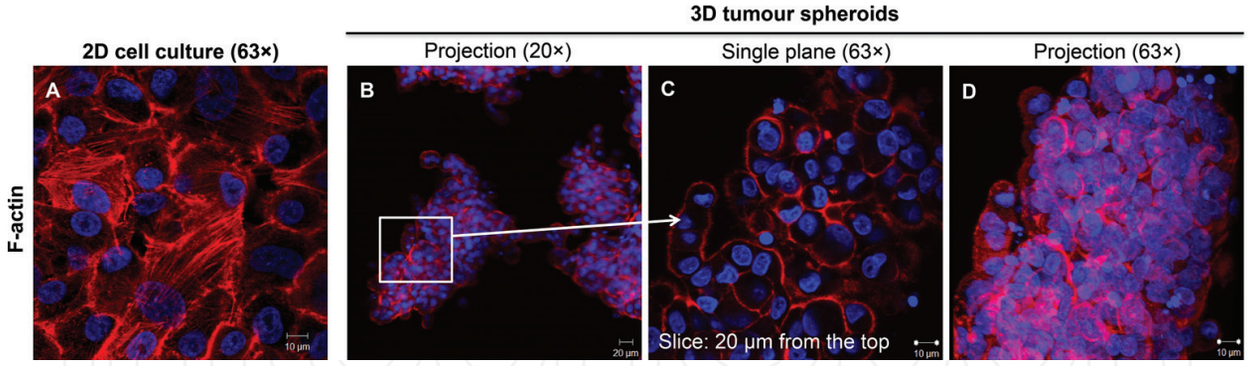

Figure 5. LSCM images of A549 cells cultured in (A) 2D and (B–D) 3D. Cells were stained with rhodamine phalloidin (1:40 dilution) to detect F-actin filaments (in red) and Hoechst (1:400 dilution) as nuclear counterstain (in blue). Images were collected in (A, C) single-plane or (B, D) Z-stack mode with a 20× (scale bar: 20 μm) or an oil-immersion 63× (scale bars: 10 μm) objective lens. (D) Projection of Z-stack images obtained with the projection function of Zeiss LSM 5 software (61 sections, total height: 48 μm).

cells grown in 2D on glass substrates and stained for F-actin were used as control. Our protocol allowed determining that, when grown in scaffold-free 3D tumour spheroids, A549 cells showed a round cell shape and expressed cortical F-actin; in contrast, 2D cell cultures showed a cytoskeleton organised in cytoplasmic F-actin stress fibres.

4.2.1.1.2. Experimental validation: cell phenotype—expression of mesenchymal and epithelial markers

The microenvironment is known to influence the conversion of epithelial cells into mesenchymal cells in *in vitro* systems [98, 99] by a process called epithelial-to-mesenchymal transition (EMT). EMT is a critical series of events that switch early stage carcinomas into invasive malignancies. EMT is associated with the loss of epithelial cell markers and the acquisition of mesenchymal features [100, 101].

By applying our protocol for immunocytochemistry, 3D tumour spheroids formed in 96-well ULA plates were assessed for the expression of two mesenchymal markers: vimentin and fibronectin. **Figure 6** shows some representative results. In clinical trials, vimentin expression is used as a clinical marker of the response of NSCLC to chemotherapeutic agents [102], since increased expression of this protein gives an indication of tumour progression. In parallel, fibronectin expression is increased in NSCLC, enhancing the cells' invasiveness and conferring them resistance to apoptosis-inducing chemotherapeutic agents. Thus, the detection of these markers was selected during validation experiments as it finds a useful application in the preclinical drug efficacy-screening pipeline. Our immunocytochemistry could, for example, be used for characterising spheroids cultured at different time points or formed by different protocols, allowing for the selection of the most relevant *in vitro* model to be used in preclinical tests. The expression levels to be mimicked should be assessed based on patient-based, clinically relevant data.

Our immunocytochemistry protocol was also found to be applicable for the evaluation of the expression of cleaved E-cadherin and β-catenin and for the investigation of their localization in the cell body (**Figure 7A–F**). Cells with epithelial phenotypes form adherent junctions. In such junctions, β-catenin binds to the cytoplasmic tail of the protein E-cadherin. During EMT,

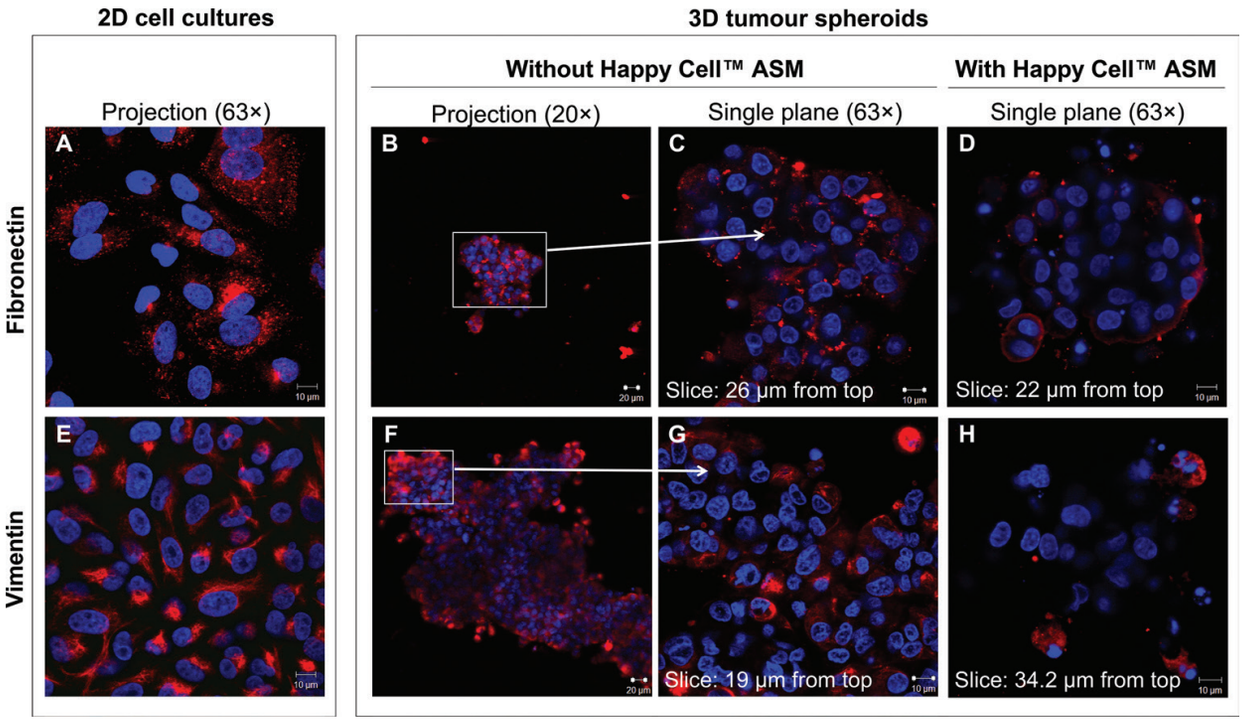

Figure 6. LSCM images of (A, E) 2D cell cultures and (B–D, F–H) 3D tumour spheroids stained for (A–D) fibronectin and (E–H) vimentin (both in red). 3D tumour spheroids were formed in ULA plates (B, C, F, G) with or (D, H) without Happy Cell™ ASM. For fibronectin detection, cells were stained with Sheep Anti-Human Fibronectin Antigen Affinity-purified Polyclonal primary IgG (1:20 dilution) and NorthernLights™ 557-conjugated Anti-Sheep secondary IgG (1:200 dilution) was used as secondary antibody. For vimentin immunocytochemistry, cells were stained with Goat Anti-Human Vimentin Antigen Affinity-purified Polyclonal primary IgG (1:20 dilution) and NorthernLights™ 557-conjugated Anti-Goat secondary IgG (1:200 dilution) was used as secondary antibody. Nuclei were counterstained with Hoechst (1:400 dilution) (in blue). (A, E) In 2D cell cultures, fibronectin showed a dotted pattern, while vimentin appeared as robust stress fibres. (B–D, F–H) Cells in 3D tumour spheroids showed cytoplasmic expression of vimentin and fibronectin, with reduced expression in centrally located cells (spheroid core). (B, F) Projection of Z-stack images obtained with the projection function of Zeiss LSM5 software (19 sections, total height: 46.77 µm). (B, F) White boxes highlight the region of the 3D tumour spheroids magnified in image (C) and (G), respectively. Scale bars: (B, F) 20 µm (20× objective lens) and (A, C–E, G, H) 10 µm (63× objective lens).

the intracellular fragment of E-cadherin (called cleaved E-cadherin) translocates into the cell nucleus. This results in the abolishment of the E-cadherin-mediated sequestering of β-catenin in the cytoplasm and the translocation of β-catenin to the cell nucleus. Co-localization studies were possible on an example set of LSCM images acquired from specimens prepared as described above. Such studies showed that cleaved E-cadherin and β-catenin were mainly localised in the cells' nuclei when A549 cells were cultured as 3D tumour spheroids in 96-well ULA plates without Happy Cell™ ASM (**Figure 7J**).

Tight junctions (TJs) are also involved in cell adhesion and lung cancer development [103]. In particular, occludin plays a critical role in defining the cellular phenotypes in solid tumours [104]: while epithelial cell phenotypes express occludin, cells with mesenchymal phenotypes downregulate occludin expression, resulting in enhanced cellular invasiveness and motility and thus promoting tumorigenic and metastatic properties of tumour cells [101]. **Figure 8** shows representative LSCM images demonstrating that the immunocytochemistry protocol described in this study allowed evaluating the expression of occluding in 3D tumour spheroids.

http://dx.doi.org/10.5772/intechopen.69447

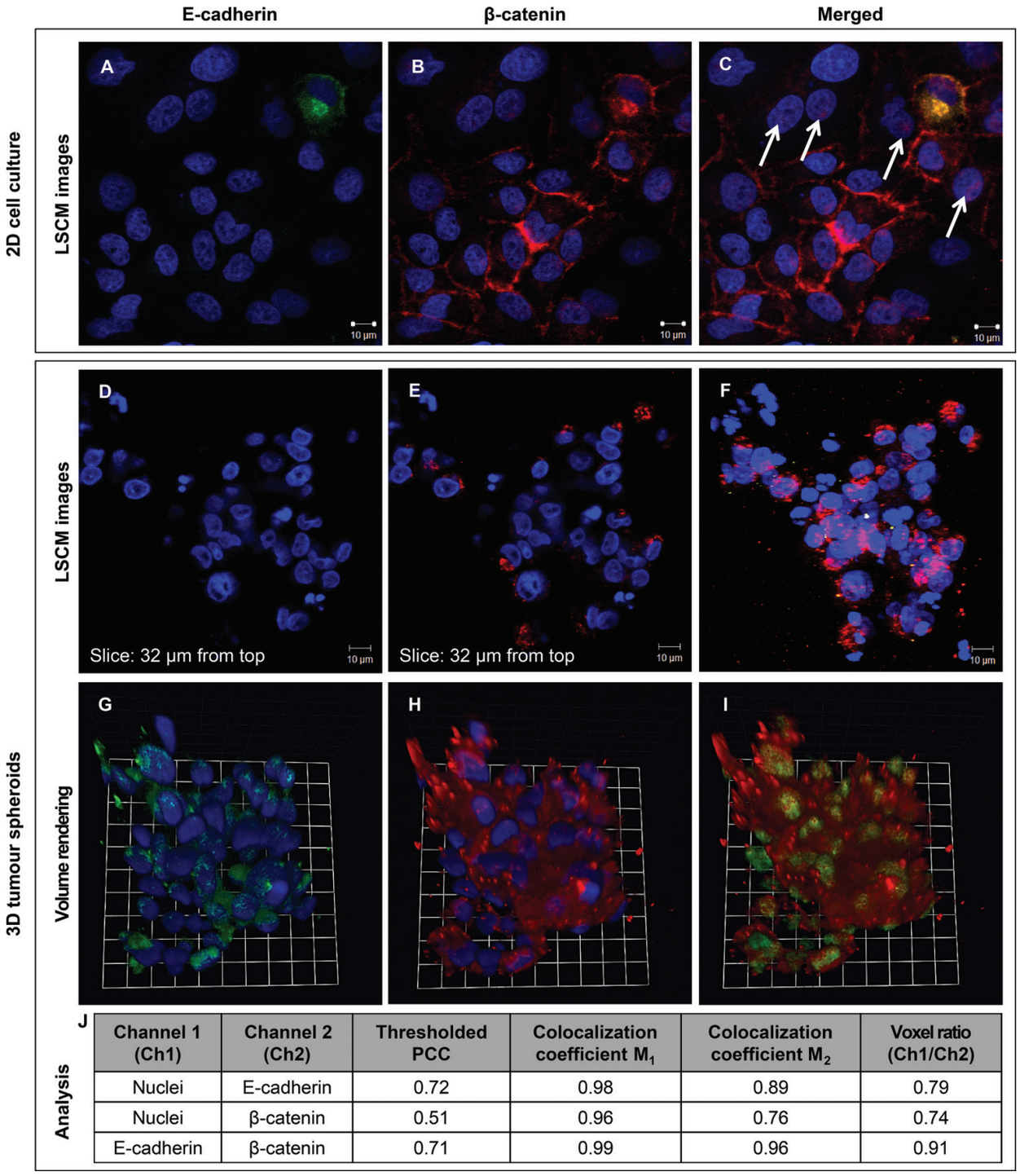

Channel 1 (Ch1)	Channel 2 (Ch2)	Thresholded PCC	Colocalization coefficient M_1	Colocalization coefficient M_2	Voxel ratio (Ch1/Ch2)
Nuclei	E-cadherin	0.72	0.98	0.89	0.79
Nuclei	β-catenin	0.51	0.96	0.76	0.74
E-cadherin	β-catenin	0.71	0.99	0.96	0.91

Figure 7. LSCM images of (A-C) 2D cell cultures and (D–F) 3D tumour spheroids stained for cleaved E-cadherin (in green), β-catenin (in red) and nuclei (in blue). 3D tumour spheroids were formed in ULA plates without Happy Cell™ ASM. A549 cells were stained with FITC-conjugated Mouse Anti-Human E-cadherin IgG (1:70 dilution), Mouse Anti-Human β-catenin primary IgG (1:50 dilution) and Hoechst nuclear counterstain (1:400 dilution). As secondary antibody, Alexa Fluor 568-conjugated Goat anti-Mouse secondary IgG (1:1000 dilution) was used. (C) White arrows highlight nuclear translocation of β-catenin. (C, F) Projection of Z-stack images obtained with the projection function of Zeiss LSM 5 software (54 sections, total height: 57.32 µm). Scale bars: 10 µm (63× objective lens). (G–I) Volume rendering of representative Z-stack LSCM images of 3D tumour spheroids and (J) co-localization studies. (G–I) Volume rendering was obtained with the Volocity software. Scale bar: 1 unit = 12 µm.

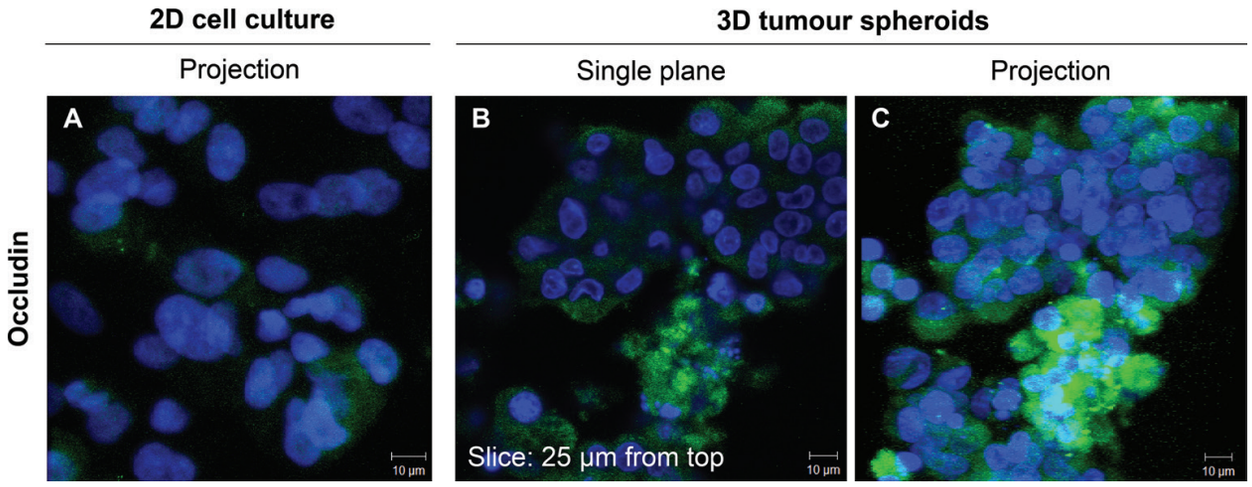

Figure 8. LSCM images of (A) 2D cell cultures and (B–C) 3D tumour spheroids stained for occludin with FITC-conjugated Mouse Anti-Human Occludin IgG (1:50 dilution) (in green) and for nuclei with Hoechst (1:400 dilution) (in blue). 3D tumour spheroids were formed in ULA plates, without Happy Cell™ ASM. (A, C) Projection of Z-stack images were obtained with the projection function of Zeiss LSM 5 software (77 sections, total height: 76 µm). (A–C) Scale bars: 10 µm (63× objective lens).

4.2.1.1.3. Experimental validation: tumour differentiation—expression of Connexin-43 (Cx-43)

Cx43 represents one of the predominant gap junction proteins; its down-regulation is associated to poorly differentiated NSCLC, as showed *in vitro* and in human tissue [105]. Thus, Cx43 is a cellular marker of the tumour differentiation. **Figure 8** shows representative micrographs of fixed 3D tumour spheroids labelled with an anti-Cx43 antibody following our protocol described above (**Figure 9**).

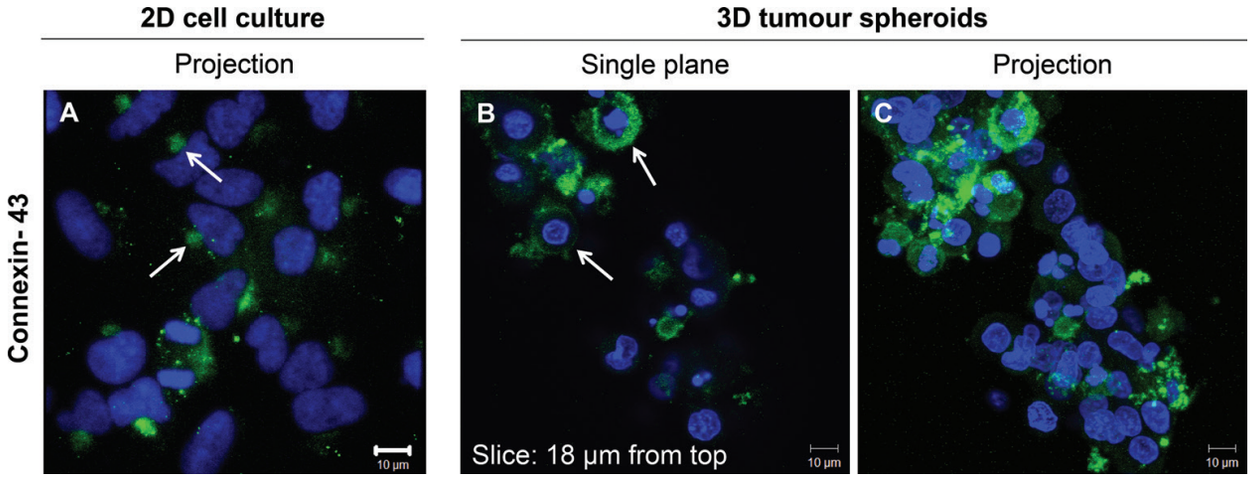

Figure 9. LSCM images of (A) 2D cell cultures and (B–C) 3D tumour spheroids stained with Alexa Fluor 488-conjugated Monoclonal Mouse Anti-Human Connexin-43 IgG (1:50 dilution) and Hoechst nuclear counterstain (1:400 dilution). 3D tumour spheroids were formed in ULA plates, without Happy Cell™ ASM. Arrows highlight (A) expression of connnexin-43 plaques in 2D cell cultures and (B) cortical expression of connexin-43 in 3D tumour spheroids. (C) Projection of Z-stack images were obtained with the projection function of Zeiss LSM5 software (46 sections, total height: 58.5 µm). (A–C) Scale bars: 10 µm (63× magnification).

http://dx.doi.org/10.5772/intechopen.69447

4.2.1.2. Advanced microscopy

The protocol presented within this section contains a series of detailed steps that allow examining the morphology of cultured cells subsequent to 3D growth by advanced microscopy, such as, for example, scanning electron microscopy (SEM) or He-ion microscopy (HIM).

It is widely accepted that the preparation methods of biological specimens for SEM/HIM imaging can introduce artefacts. To avoid this and to preserve the cells' architecture, we recommend employing a drying method using hexamethyldisilazane (HMDS). HMDS represents a cost- and time-efficient alternative to critical point drying (CPD) in the preparation of cells for electron microscopy imaging [106, 107].

A. Dehydration of fixed 3D tumour spheroids:

- Following fixation, immerse samples in PBS to remove excess fixative for 10 min—all steps are carried out at room temperature.
- Gently aspirate the 3D tumour spheroids with a 1000 μL tip and transfer them on microscope glass slides previously marked with a liquid-repellent slide marker pen for staining procedures.

  Please note: the use of a 1000 μL tip is necessary to avoid perturbation of the original 3D spheroids architecture.
- Add an excess of 30% ethanol (EtOH) to samples, and leave them to equilibrate for 10 min.
- Discard excess liquid. Excess solutions should be discarded by gentle pipetting (avoid vacuum-pipetting) out the liquids, making sure that 3D tumour spheroids (visible by naked eye as small white spots after addition of EtOH) are not accidentally aspirated during this step.
- Repeat previous steps with 50, 70 and 90% EtOH, and leave to equilibrate for 10 min for each solution—discard solutions after each incubation.
- Add an excess of absolute EtOH and leave to equilibrate for 20 min—discard excess liquid. Repeat this step twice, discarding the solution after each incubation.

B. Chemical drying of dehydrated 3D tumour spheroids:

- Add an excess of 30% HDMS and leave to equilibrate for 5 min. Handle HDMS with care. HDMS is a flammable liquid and vapour. It is harmful if swallowed, inhaled or absorbed through skin. It causes severe irritation or burns to skin, eyes and respiratory tract. Avoid contact with eyes and skin. Avoid breathing vapours. Wear goggles, gloves and protective clothing. Use only with adequate ventilation. Wash hands thoroughly after handling. Avoid prolonged or repeated exposure.
- Discard excess solution.
- Add an excess of 60% HDMS and leave to equilibrate for 5 min.
- After discarding the solution, add an excess of pure HDMS and equilibrate for 10 min.
- Remove excess liquid and dry in a chemical fumehood overnight.

4.2.1.2.1. Experimental validation: imaging of 3D architecture, cell membrane texture and cell shape by HIM

He-ion microscopy (HIM) is an advanced imaging technique in which a focused beam of He^+ ions is directed onto the sample surface, which liberates secondary electrons that are collected forming detailed images of the sample surface topography [108]. In biomedical sciences, HIM offers various advantages over conventional SEM imaging, such as a high spatial resolution (with better material contrast and improved depth of focus) and the ability to image uncoated, non-conductive samples without the deposition of a metal (or other conductive) overcoat [109, 110], which can indeed reduce and/or completely mask cell surface details [111]. This opens up a whole new range of surface details in biological specimens that can be examined rapidly and with less risk of artefacts. HIM accuracy can be indeed exploited to image the shape, membrane texture, membranous projections and 3D architecture of 3D tumour spheroids with unsurpassed image quality and detail.

Our protocol for advanced microscopy was found valuable for capturing HIM images of 3D tumour spheroids formed without Happy Cell™ ASM in 96-well ULA plates (**Figure 10**).

4.2.2. Molecular analysis

Because of the central role of proteins in understanding cancer cells responses, it is often valuable to be able to extract, purify and quantify the expression of specific proteins. Thus, we developed an easy-to-use protocol outlining the steps necessary for the extraction of total protein from 3D tumour spheroids.

A. Collect 3D tumour spheroids:

- Aspirate growth media and 3D tumour spheroids formed with a 1000 μL pipette from each well and collect them in a 20 mL tube.

  Please note the use of a 1000 μL tip is necessary to avoid perturbation of the original 3D spheroids architecture
- Centrifuge at 5000 rpm at room temperature (25°C) for 20 min.

B. Total protein extraction:

- Aspirate the supernatant and re-suspend the cell-pellet with 1.5 mL of PBS.
- Centrifuge at 5000 rpm at room temperature (25°C) for 20 min.
- Aspirate the supernatant and re-suspend the cell-pellet in lysis buffer.
- After addition of the lysis buffer, mix energetically to favour disaggregation of 3D tumour spheroid-pellet.
- Proceed with standard immunoblotting.

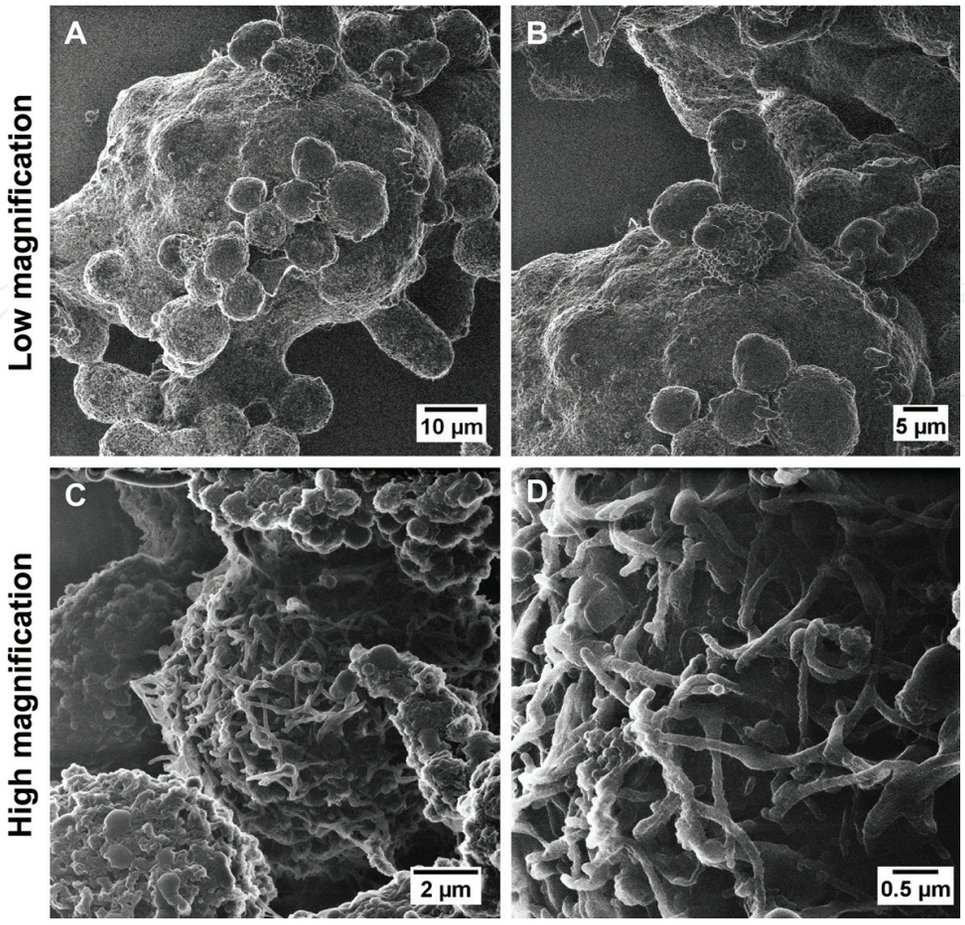

Figure 10. HIM images of A549 cells forming 3D tumour spheroids in ULA plates. The three-dimensional architecture of the spheroids can be appreciated at low magnification (A–B), while the presence of unique membrane ruffles and a multitude of filopodia and lamellipodia on the cells surface can be detected when imaging at high magnifications (C–D). Samples were imaged using an accelerating voltage of 30 kV. The working distance was 8 mm and a 10 μm aperture. The probe current was between 0.5 and 1.5 pA. Images were acquired by collecting the secondary electrons emitted by the interaction between the He-ion beam and the specimen with an Everhart-Thornley detector (part of the He-ion microscope system). The image signal was acquired in a 32- or 64-line integration to each contributing line of the image. Scale bars: (A) 10 μm, (B) 5 μm, (C) 2 μm and (D) 0.5 μm.

4.2.2.1. Experimental validation: Western Blot of cell junctions

Validation data were obtained using our protocol to extract protein from 3D tumour models cultured in Happy Cell™ ASM in Nunc® low-cell binding plates (24-well format), as confirmation of the molecular fingerprinting of the 3D tumour spheroids. Western blotting, a gold-standard technique in protein detection and quantification, was used for evaluating the expression in 3D tumour spheroids of (i) adherent junctions (namely, full-length protein E-cadherin and β-catenin) and (ii) TJs, such as occluding, zonula occludens-1 (ZO-1) and ZO-3. Cell lysis and Western blotting were performed following previously optimised in-house published protocols [112]. The results obtained (shown in **Figure 11**) demonstrated the expression of full-length E-cadherin and β-catenin. It should be noted that cells cultured in 3D spheroids showed nuclear translocation of cleaved E-cadherin (**Figure 7**) as well as

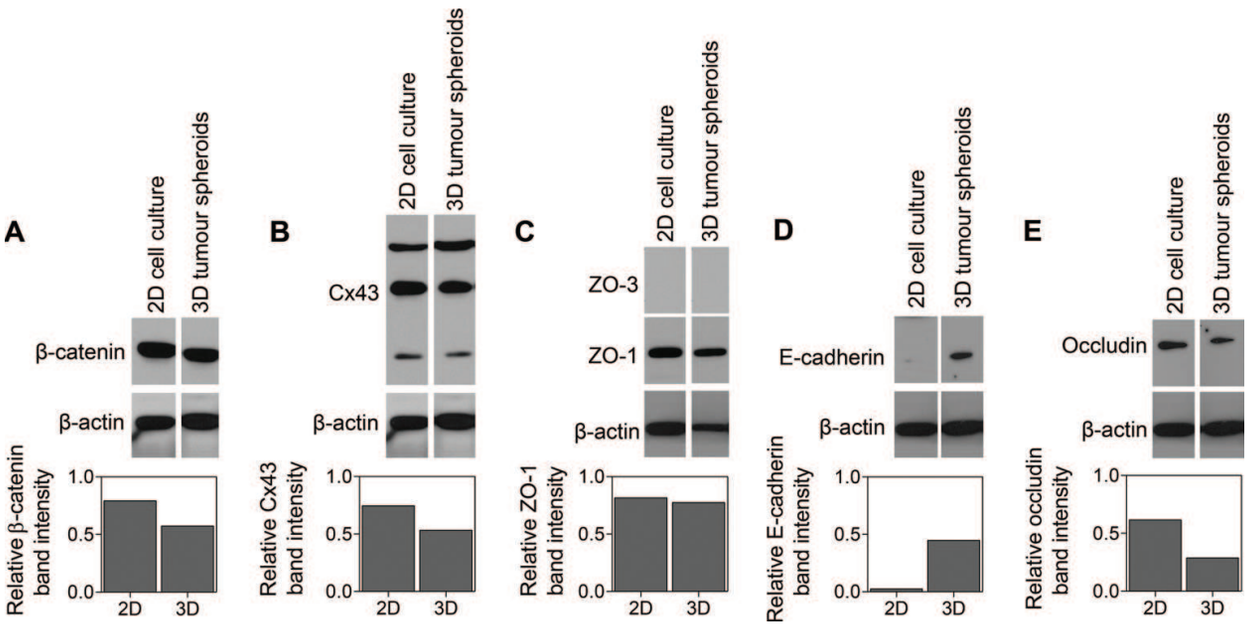

Figure 11. Western blot of (A) β-catenin (92 kDa), (B) Connexin-43 (19, 31 and 59 kDa), (C) ZO-3 (140 kDa) and ZO-1 (220 kDa), (D) full-length protein E-cadherin (135 kDa), (E) occludin (65 kDa), and relative bands intensities normalised on the β-actin bands intensity. 2D cultures and 3D tumour spheroids were lysed following the protocol described—the lysates were resolved by SDS-PAGE and after Western blotting were probed for the various proteins.

the expression of full-length E-cadherin (**Figure 11**): co-expression of these two forms of the E-cadherin protein is in fact possible during intermediate steps of the EMT process. In addition, Western blot showed that occluding and ZO-1 were expressed, whereas ZO-3 was not. For forming functional TJs, the transmembrane components of occludin need to interact with at least one ZO protein [113]. Our results seemed to suggest therefore that functional TJs might have been formed in 3D tumour spheroids.

4.3. Protocol for the evaluation of biological responses in 3D tumour spheroids

Exposure of 3D tumour spheroids formed with our protocol to drugs or nanomedicine candidates resulted very simple, as the spheroids could be exposed to the tested compounds/nanocarriers by their direct addition in the media, as conventionally used in 2D cell culturing protocols. In order to quantify the cellular responses to the drugs/nanocarriers tested, we developed protocols based on commercially available assays that are routinely applied to monitor intracellular activity in 2D monolayer cell cultures.

Various techniques are used to characterise the effect of anticancer agents on 3D tumour spheroids, as described in a recently published review [95]. In general, monitoring of spheroid integrity by phase contrast imaging is still the most popular technique to evaluate the cytotoxic effects of drugs. Spheroid growth delay, a classical analytical endpoint, is most frequently calculated as the difference between treated and untreated spheroids to reach a particular volume and has recently been proposed for standardised spheroid screening [114]. However, with respect to clinical relevance, loss of spheroid integrity may not result from total tumour cells destruction, as spheroid integrity does not necessarily reflect the presence

http://dx.doi.org/10.5772/intechopen.69447

of viable cells. Therefore, quantification of cell survival after treatment is desirable. Our protocols for conventional and high-throughput assays can be used for visualising and monitoring the viability of the cell population in the spheroids. Thus, they allow for the investigation of (i) the therapeutic efficacy of tested chemotherapeutic agents, (ii) the toxicity of nanocarriers and/or (iii) the efficiency in delivering anticancer treatments by means of nanocarriers.

4.3.1. Conventional assays

Standardised protocols, which do not require further optimization depending on the rate of cell growth or the cell culturing substrate used, are described in detail for the live/dead cytotoxicity and trypan blue exclusion assays in the following sections.

A. Live/dead cytotoxicity assay in 3D tumour spheroids:

- At the desired time point, harvest cells by gentle pipetting 100 μL/well media. This operation cannot be performed with vacuum pipettes, to avoid accidental aspiration of the 3D tumour spheroids formed.
- Add the pre-warmed staining solution (100 μL/well) to the wells. Staining solution is prepared as recommended in the supplier's protocol.
- Incubate for 45 min at room temperature in the dark.
- Gently aspirate the 3D tumour spheroids with a 1000 μL tip and proceed to analysis. Please note: the use of a 1000 μL tip is necessary to avoid any potential perturbation in the spatial localization of live/dead cells.
- Please note that it is not possible to carry out analysis on stored specimens.

B. Trypan blue exclusion assay in 3D tumour spheroids:

- Aspirate growth media and 3D tumour spheroids from each well with a 1000 μL pipette and collect them in a 20 mL tube. Please note the use of a 1000 μL tip is necessary to avoid perturbation of the original 3D spheroids architecture, triggering any potential cell death.
- Centrifuge at 3000 rpm at room temperature (25°C) for 5 min.
- Aspirate the supernatant and re-suspend the cells with 1 mL of PBS.
- Add 100 μL of trypan blue solution (0.4%) to 1 mL of cells.
- After addition of the trypan blue solution, mix energetically to favour disaggregation of 3D tumour spheroids.
- Load a haemocytometer or a cell counter slide with the stained cell suspension.
- Immediately count the number of blue stained cells and the number of unstained cells under a low magnification microscope or with an automatic cell counter.
- To calculate the percentage (%) of live cells use Eq. (1):

$$\% \text{ live cells} = \left[1 - \frac{\text{number of stained cells}}{\text{number of total cells}}\right] \times 100 \quad (1)$$

4.3.1.1. Experimental validation: therapeutic efficacy of Paclitaxel in 3D tumour spheroids

In the validation of our protocol, the live/dead cytotoxicity assay was integrated with LSCM. 3D tumour spheroids were formed without Happy Cell™ ASM in 96-well ULA plates. 3D tumour spheroids were then exposed to Paclitaxel (0.03 mM) for 24 and 72 h, and the percentage of live cells was compared to the paired negative (untreated cells) and positive controls (cells treated with 70% MeOH for 30 min at 37°C). Representative LSCM images of 3D tumour spheroids stained with the devised protocol for live/dead cytotoxicity assay are shown in **Figure 12**. Analysis of LSCM images demonstrates a small (but not significant) increase in the proportion of dead cells when 3D tumour spheroids were exposed to Paclitaxel for 24 h, while the size of the spheroids appeared reduced following exposure at both time points. The treatment with 70% MeOH provided the expected positive control outcome.

Further to this, the viability of 3D tumour spheroids exposed to Paclitaxel (0.03 mM) for 24 and 72 h was evaluated by means of the trypan blue exclusion assay protocol. Quantitative data are reported in **Figure 13** as the average ± standard deviation ($n_{replicates} \geq 2$). Exposure to Paclitaxel for 24 h resulted in a significant reduction in cell viability in 3D tumour spheroids, although cell viability increased after 72 h treatment. This result might be related to the well-known ability of 3D tumour spheroids to mimic drug resistance phenomena [115, 116], which has been observed *in vivo*. As expected, treatment with 70% MeOH resulted in a significant reduction of live cells as positive control sample.

4.3.1.2. Experimental validation: cytotoxicity of nanocarriers in 3D tumour spheroids and therapeutic efficacy of anticancer agents delivered by nanocarriers

3D tumour spheroids were formed without Happy Cell™ ASM in 96-well ULA plates and exposed to gold nanoboxes (Au-1) and its nanomedicine form consisting of a multi-layered nanomaterial made of the same gold core (Au-1) coated with Paclitaxel-encapsulated gelatine (Au-2). Full characterisation of these nanomaterials is provided in a previous publication of the authors [117]. 3D tumour spheroids were exposed to Au-1 and Au-2 for 24 or 72 h. The experimental design included a negative control (untreated cells) and a positive control (cells treated with 70% MeOH for 30 min at 37°C). Representative LSCM images of 3D tumour spheroids stained with the live/dead cytotoxicity assay protocol are shown in **Figure 14**. Analysis of such images allowed concluding that Au-1 did not produce any significant variation in the cell viability following 24 and 72 h exposure, whereas 72 h exposure to Au-2 resulted in a reduction of the total amount of live cells in the 3D tumour spheroids.

Trypan blue exclusion assay was carried out in parallel experiments, where 3D tumour spheroids formed in 96-well ULA plates were exposed to Au-1 for 24 and 72 h. The quantitative results are reported in **Figure 15** as average ± standard deviation ($n_{replicates} \geq 2$). The assay confirmed that such nanocarriers did not cause any cytotoxicity when incubated with 3D tumour spheroids for 72 h.

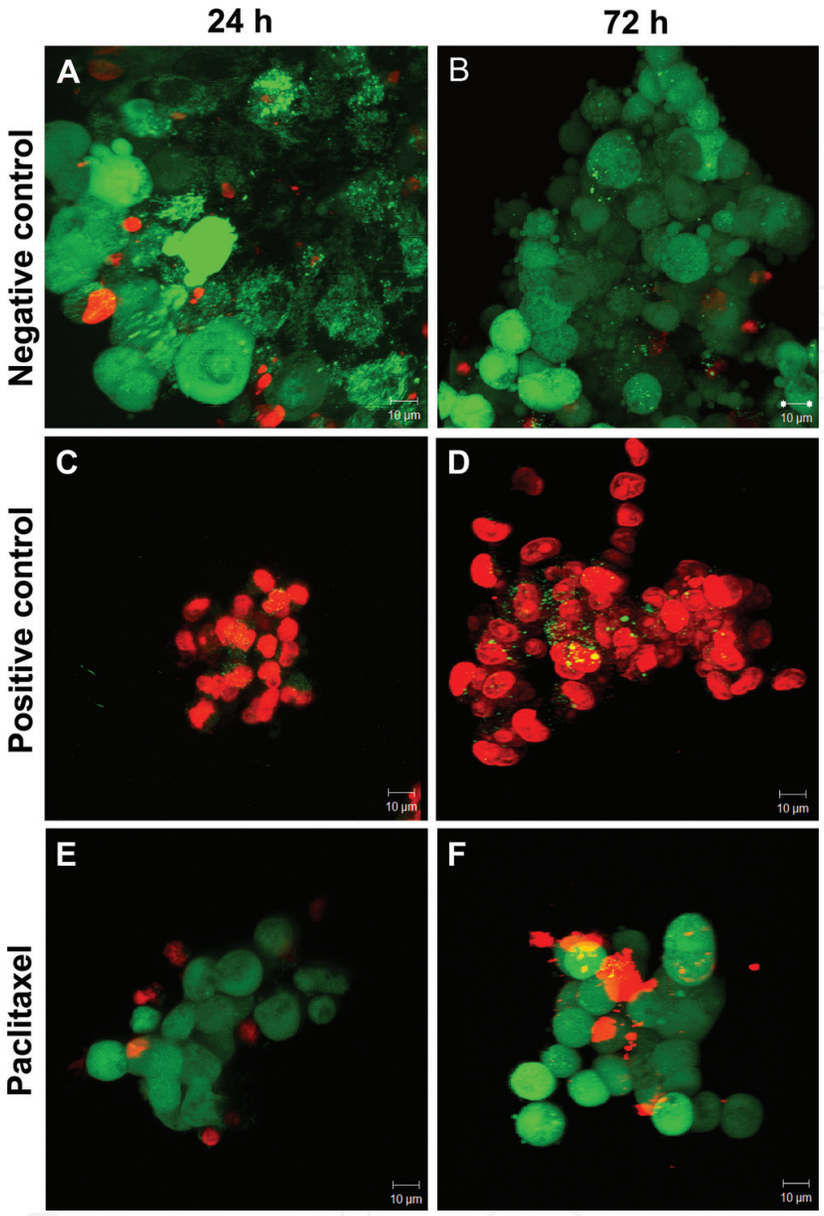

Figure 12. LSCM images of 3D tumour spheroids stained for live (calcein AM; 1:500 dilution; in green) and dead (ethidium homodimer-1; 1:300 dilution; in red) cells after 24 and 72 h exposure to Paclitaxel (0.03 mM). Negative (untreated 3D tumour spheroids) and positive (3D tumour spheroids treated with 70% MeOH for 30 min) controls are also reported. Scale bars: 10 µm (63× objective lens).

4.3.2. High-throughput assays

The setup based on high-throughput flow cytometry is described below. This setup could be easily integrated into a standard large-scale drug-testing routine. The setup requires a small number of spheroids and a limited amount of drug/nanomedicine candidate, and it can integrate many analytical endpoints. Since spheroid dissociation is carried out during the sample preparation steps, this assay is suitable for all spheroid size ranges that may be examined when comparing treated and untreated spheroids.

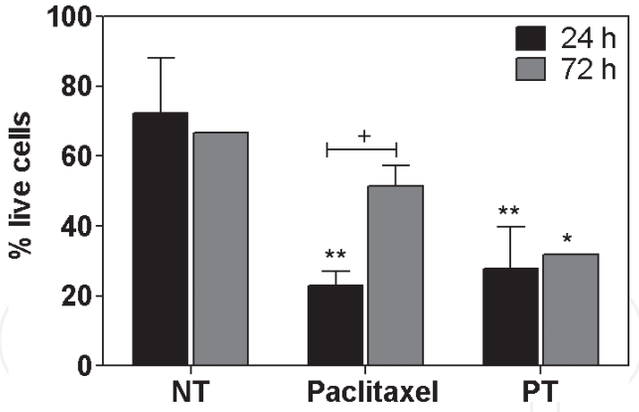

Figure 13. Percentage (%) of live cells in 3D tumour spheroids grown in ULA plates without Happy Cell™ ASM and exposed to Paclitaxel (0.03 mM) for 24 and 72 h. Untreated (negative control or NT) and 70% MeOH-treated (positive control or PT) 3D tumour spheroids were also included in the experimental design. Stained and unstained cells were counted by a Countess™ cell counter. For the statistical analysis, a two-way analysis of variance (2-way ANOVA) followed by Bonferroni post-test analysis was carried out (GraphPad Prism 5 Software Inc., USA). $p < 0.05$ was considered statistically significant. The symbols (*) and (**) indicate $p < 0.05$ and $p < 0.01$, as compared to NT. The symbol (+) indicates $p < 0.05$ as compared to 24 h.

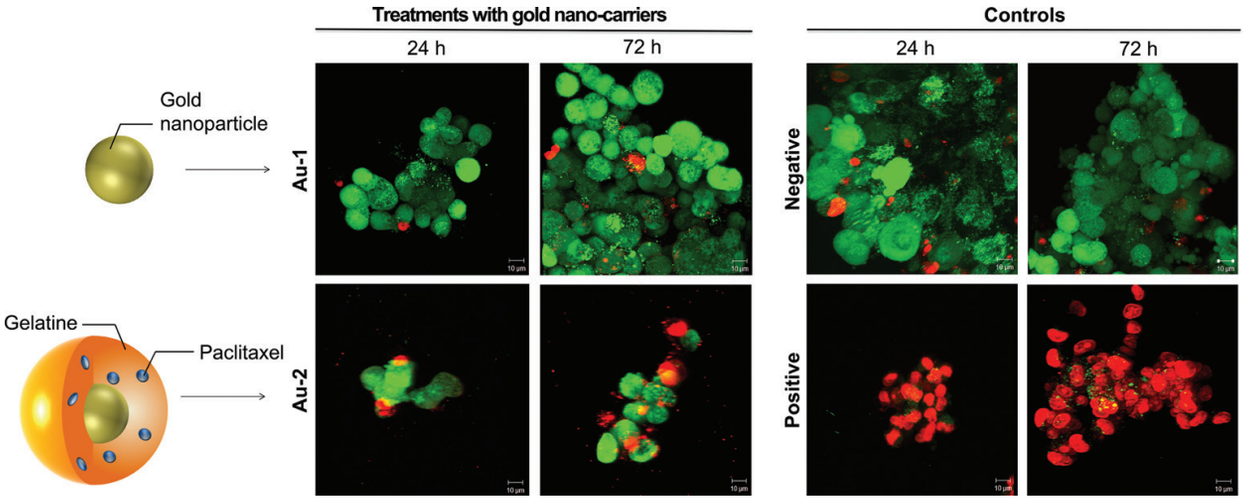

Figure 14. LSCM images of 3D tumour spheroids stained for live (calcein AM; 1:500 dilution; in green) and dead (ethidium homodimer-1; 1:300 dilution; in red) cells after 24 and 72 h exposure to a gold nanocarrier (Au-1) or Paclitaxel-loaded, gelatine-coated gold nanocarriers (Au-2). Negative (untreated 3D tumour spheroids) and positive (3D tumour spheroids treated with 70% MeOH for 30 min) controls are also reported. Scale bars: 10 μm (63× objective lens).

A. Sample preparation:

- At the desired time point, aspirate growth media and 3D tumour spheroids from each well with a 1000 μL pipette and collect them in a 20 mL tube.
- Centrifuge at 1650 rpm at room temperature (25°C) for 5 min.

B. Assay:

- Perform the cell staining with the kit chosen according to the manufacturer's protocol, and run the sample in the flow cytometer.

- Special considerations: please note that the assay kit used in this study does not require a step for disaggregating the 3D tumour spheroids in a single cell suspension, as lysis of cells is performed during the assay. An additional step might be required if a different kit is used.

4.3.2.1. Experimental validation: changes in cell cycle following exposure to Paclitaxel

Example data were obtained using the protocol described above to quantify the cell cycle changes in 3D tumour spheroids exposed to Paclitaxel (0.03 mM) for 24 h. Stained nuclei were visualised using the SSC-H vs FSC-H scatter plot and a gate (P1) was applied to exclude debris at lower scatter intensities. Aggregate exclusion gating (P2 in P1) via doublet discrimination was performed on the P1 population using the FL2-H vs FL2-A scatter. Finally, analysis of the cell cycle stage for G0/G1, S and G2/M phase was carried out by manual gating on the FL2-H histogram. A minimum of 10,000 events was collected in the (P2 in P1) gate and visualised on the FL2-H histogram. Data are presented in **Figure 16** as percentage (%) cell population in (P2 in P1) and expressed as average ± standard deviation ($n_{test} = 2$).

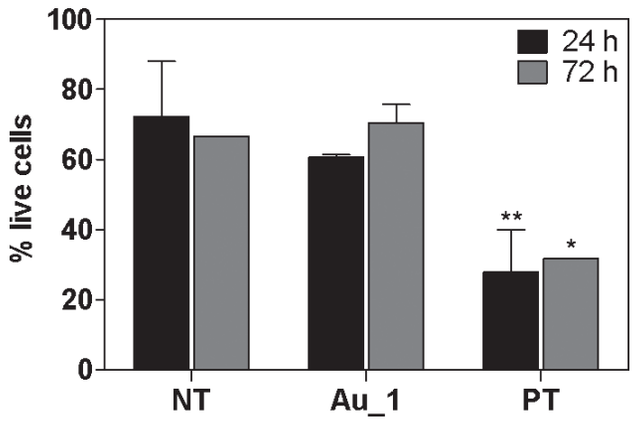

Figure 15. Percentage (%) of live cells in 3D tumour spheroids grown in ULA plates after exposure to gold nanoparticles for 24 and 72 h. Untreated (negative control or NT) and 70% MeOH-treated (positive control or PT) 3D tumour spheroids were also included in the experimental design. Stained and unstained cells were counted by a Countess™ cell counter. For the statistical analysis, a two-way ANOVA followed by Bonferroni post-test analysis was carried out (GraphPad Prism 5 Software Inc., USA). $p < 0.05$ was considered statistically significant. The symbols (*) and (**) indicate $p < 0.05$ and $p < 0.01$ as compared to NT.

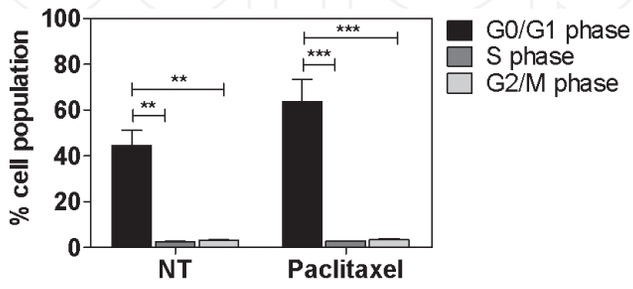

Figure 16. Percentage (%) of cell population in the G0/G1, S and G2/M phases after exposure to Paclitaxel (0.03 mM) for 24 h. cells were stained with the BD Cycletest™ Plus DNA Reagent Kit and analysed using BD Accuri™ C6 flow cytometer. Data are shown as average ± standard deviation ($n_{replicates} = 2$). For the statistical analysis, a two-way ANOVA followed by Bonferroni post-test analysis was carried out (GraphPad Prism 5 Software Inc., USA). $p < 0.05$ was considered statistically significant. The symbols (**) and (***) indicate significant changes ($p < 0.01$ and $p < 0.001$, respectively) compared to the G0/G1 phase.

Our data showed an increase in the percentage cell population in G0/G1 phase after 24 h treatment with Paclitaxel. This anticancer drug is known to inhibit the mitotic spindle formation, thus blocking the progression of mitosis and triggering apoptosis or reversion to the G-phase of the cell cycle without cell division. The results presented in **Figure 16** reflect the mechanism of action of the drug under investigation, and validate the trypan blue exclusion assay results, showing an increased cell death following 24 h exposure to Paclitaxel (**Figure 13**).

5. Authors' perspective

Since 2006, when a simple method to generate non-adherent 3D tumour spheroids for potential high-throughput toxicity analysis of drug compounds was firstly reported [118], several methods have been developed to generate scaffold-free 3D tumour spheroids for drug discovery. These methods share the common feature of promoting cell-cell coupling by resisting cell-substrate interactions. They can be grouped into four main methodological categories: (i) hanging drop [85, 119, 120]; (ii) cell culture on non-adherent surfaces that effectively inhibits cellular attachment, such as (poly-HEMA)-coated plates [121, 122], low-binding plates [123, 124], ultra-low attachment (ULA) plates [125] or micro-patterned plates [126, 127]; (iii) microcarrier systems [128] and (iv) rotation-based culturing techniques, such as spinner flasks [129] and rotary cell culture systems [130, 131]. Formation of scaffold-free heterotypic multicellular 3D spheroids has likewise been extensively reported [132]. Nevertheless, when transferring drug testing to the third dimension, the limited ability to image, process and automate assays performance in 3D tumour spheroids still remains the main barrier for the adoption of these 3D culture techniques for routine preclinical drug development studies [133].

To the best of our knowledge, the main commercial approaches to the automation of scaffold-free 3D cell culturing techniques are InSphero GravityPLUS™ Hanging Drop system and GravityTRAP™ ULA plates, 3D Biomatrix's Perfecta3D™ hanging drop multi-well plates, Global Cell Solutions magnetic microcarrier-based GEM™ and PolyGEM™ systems, and Happy Cell™ ASM. Although each method has certain advantages, the challenges that these approaches still pose for automation are well-documented [24]. In detail, limitations are posed to imaging due to *Z*-axis resolution, image depth and light scattering [134], although advances have been recently made in this field [135] by, for example, introducing additional post-processing treatments of 3D spheroids with Scale reagent [136]. The main consequence is that most studies on 3D tumour spheroids are carried out at low resolution by light microscopy and immunohistochemistry, or at the single-cell level by multiphoton microscopy or spectroscopic imaging/mapping techniques [137]. These techniques however are not compatible with high-throughput screening. In addition to these technical aspects, most of the commercially available products for scaffold-free 3D cell culture are not accompanied by technical documentation or peer-reviewed scientific publications describing the specific protocols that need to be used for drug discovery applications. For many of the products mentioned above, users and operators are left with the burden of re-optimising the working protocols to their specific needs. For instance, it is known that cells in Happy Cell™ ASM, a product used in this study, form discrete populations within the wells of 96-well low-cell binding plates provided by the same supplier

http://dx.doi.org/10.5772/intechopen.69447

and, during continued culture, they assemble into spheroids. However, no information is provided on: (i) the size of the 3D tumour spheroids formed in the multi-well plates supplied by Biocroi Ltd itself; (ii) the size of the 3D tumour spheroids obtained if using multi-well plates purchased from different commercial sources and compatible with high-throughput screening assays and (iii) how to standardise and homogenise the size of 3D tumour spheroids. Similarly, according to the manufacturer, protocols for the formation, maintenance and harvesting of 3D tumour spheroids formed in 3D Biomatrix's Perfecta3D™ hanging drop multi-well plates should be optimised by each user[138–140]. Such uncertainties are indeed strongly hindering the integration of 3D culturing technologies into the pharmaceutical industry practice.

The aim of this study was to develop practical and technical solutions filling such gaps of standardisation, focusing on screening applications that are achievable without expensive robotic equipment and that could be employed in many research labs. Happy Cell™ ASM was selected as the least characterised product, whereas low-binding/ULA multi-well plates were chosen as they are the most common substrates currently used for forming 3D tumour spheroids. Human adenocarcinoma cells (A549 cell line) were selected as a relevant model for developing technical protocols with translational potential in the drug development pipeline: all results presented here are based on such cell line. The A549 cell line is considered one of the closest cell line mimicking the human epithelial alveolar model [141], and a physiologically relevant *in vitro* model of NSCLC [142], which is the most prevalent form of human lung cancer originating from epithelial cells. A549 cells are also an established cell line for anticancer drugs discovery and screening [143] and it has proven to be a robust cell line/alveolar model for several previous nanomaterial-based studies [112, 117, 144–148]. Unlike other studies on A549 cells [118, 149–151], the formation of our 3D tumour spheroids did not require architecturally complex scaffolds or reconstitute basement membrane that could circumvent some applications, such as drug delivery and assays performance.

The protocols developed can be grouped in three categories (in dark blue in **Figure 1**). For each of the identified categories, experimental validation was carried out and is reported in the form in which they have been used in our lab, namely forming 3D tumour spheroids and incorporating them into a 3D co-culture model, characterising the markers expressed by 3D tumour spheroids, and testing an anticancer drug or gold nanocarriers.

Our protocol allowed cell aggregation and spheroids formation in standard commercially available multi-well plates, thus meeting the pharmaceutical industry requirements [133]. Formation of 3D tumour spheroids was easily controlled by tuning specific parameters (i.e. the initial cell aggregation and cells adhesion to the substrate). 3D structure and mechanical robustness are mandatory requirements to allow the translation and implementation of 3D tumour spheroids into a primary drug-testing routine. Without these features, in fact, the pathophysiological gradients developed in genuine tumour spheroids cannot be mimicked [94]. Unfortunately, some so-called spheroids in the literature are no more than loose aggregates that easily detach; they cannot be manipulated or transferred and they show lack cell-cell interactions [23]. Our experimental data demonstrated that only 3D tumour spheroids formed in 24-well low-cell binding plates and ULA plates were mechanically robust (**Figure 3**). 3D tumour spheroids formed in these cell culture plates could be easily transferred

onto different substrates for further specific analysis (e.g. immunofluorescence staining and imaging), showing a beneficial advantage over other multi-well cell plates.

As heterotypic cell interactions are key for the function of certain tissues, co-cultures including multiple cell types are another means of increasing relevance to *in vivo* scenario [152]. A protocol for forming 3D co-culture tumour models was therefore developed. Various examples of spheroid co-culture approaches are reported in the literature [153] including, but not limited to: (i) mixed spheroids, mimicking, for example, lung cancer [154]; (ii) tumour spheroids cultured on fibroblast monolayers as model of colon carcinoma [155, 156] or breast cancer [157] and (iii) tumour spheroids co-cultured with pre-established fibroblast spheroids for creating *in vitro* models of breast cancer [158–160]. Mixed spheroids are the most widely used approach. In this approach, however, the histo-morphology and cellular distribution cannot be accurately controlled by the end-user, resulting in not-homogenous (and not replicable) models, even if identical cell numbers and harmonised culture protocols are used. These models have therefore limited application as drug screening models in the pharmaceutical industry. Thus, in our study a co-culture approach in which tumour spheroids were plated onto a fibroblast monolayer was preferred. Fibroblasts were selected as these cells represent a major portion of the tumour stroma in carcinomas, and they can promote cancer progression and invasion [161, 162]. Confocal images of the 3D co-culture models formed in this study demonstrated the successful attachment of 3D spheroids of A549 cells to the fibroblast monolayer (**Figure 4**), suggesting interaction among the different cell types.

Since the presence or extent of certain tumour characteristics, such as those associated to EMT, are likely to affect drug response, it is essential to extensively characterise the spheroid model used during drug screening. The protocols described in our study allowed a simple and economically feasible evaluation of cell markers expression (**Figures 5–10**) by means of conventional and advanced microscopy approaches. Spheroids characteristics were also assessed by Western blotting (**Figure 11**). Although not all the main features of solid cancers (such as the influence of acellular stroma and immune cells) were modelled through our formation protocols, our results demonstrated that 3D tumour spheroids did reflect many important properties of solid tumours, including the expression of specific cancer markers.

Finally, keeping in mind that one of the preferred embodiments of the protocols described herein is their application in research labs for efficacy screening of new chemotherapeutic agents and oncological nanomedicine products, cell features/responses were assessed by conventional and high-throughput assays (**Figures 12–16**). Various studies provide evidence that standard cell proliferation assays (e.g. AlamarBlue assay [163]) are not suitable for quantifying cytotoxic/cytostatic responses in 3D tumour spheroids, as they do not show a linear correlation with cell densities [164], unless properly adapted. Similarly, nanomaterials are known to interfere with many assays (e.g. MTT) [3, 165]. Our protocols based on conventional viability assays satisfied criteria, such as ease-of-use and reliability, without losing the main advantages of validated commercially available kits. A protocol for high-throughput flow cytometry was also developed, resolving time and cost issues [166]. The implementation of flow cytometry can be regarded as advantageous since this technique is widely used in clinical laboratories and can include multiple molecular read-outs and endpoints.

http://dx.doi.org/10.5772/intechopen.69447

6. Conclusions

3D tumour spheroids can allow the fast development of new effective anticancer nanomedicines without dissatisfying safety, economical and ethical issues raised by societal, healthcare and pharmaceutical industry stakeholders. However, this can be achieved only by developing clear, simple and reproducible protocols for the formation and use of 3D tumour spheroids in a way that is compatible with standard analysis techniques. The protocols described within this work offer a set of tools addressing many of the problems that need to be overcome in order to translate 3D tumour spheroids into preclinical models. The obtained data validate the developed protocols to bear a novel platform technology solving the existing bottlenecks in the arena of anticancer drug and nanomedicine products development, presented here in the form of gold nanocarriers.

Acknowledgements

This work was partially supported by the CRANN Institute (CRANN Pathfinder to DM), the EU FP7 NAMDIATREAM project (NMP-2009-LARGE-3-246479) and the Irish Research Council (IRC) Government of Ireland Postdoctoral Fellowship to DM.

The authors would like to thank Biocroi Ltd for the materials supplied free-of-charge, and Kieran Crosbie Staunton for Western blotting.

Conflict of interest

The authors declare that they have no conflict of interest.

Author details

Dania Movia[1,2] and Adriele Prina-Mello[1,2,3,4]*

*Address all correspondence to: prinamea@tcd.ie

1 Laboratory for Biological Characterization of Advanced Materials (LBCAM), School of Medicine, Trinity Translational Medicine Institute (TTMI), Trinity College, Dublin, Ireland

2 Department of Clinical Medicine, School of Medicine, Trinity Translational Medicine Institute (TTMI), Trinity College, Dublin, Ireland

3 CRANN Institute, University of Dublin, Trinity College, Dublin, Ireland

4 AMBER Centre, University of Dublin, Trinity College, Dublin, Ireland

References

[1] Shi J, et al. Cancer nanomedicine: Progress, challenges and opportunities. Nature Reviews Cancer. 2017;**17**(1):20-37. DOI: 10.1038/nrc.2016.108

[2] Moffat JG, Rudolph J, Bailey D. Phenotypic screening in cancer drug discovery—Past, present and future. Nature Reviews Drug Discovery. 2014;**13**(8):588-602. DOI: 10.1038/nrd4366

[3] Bregoli L, et al. Nanomedicine applied to translational oncology: A future perspective on cancer treatment. Nanomedicine. 2016;**12**(1):81-103. DOI: 10.1016/j.nano.2015.08.006

[4] Wicki A, et al. Nanomedicine in cancer therapy: Challenges, opportunities, and clinical applications. Journal of Controlled Release. 2015;**200**:138-157. DOI: 10.1016/j.jconrel.2014.12.030

[5] Hartung T. Look back in anger—What clinical studies tell us about preclinical work. ALTEX. 2013;**30**(3):275-291

[6] Hakanson M, Cukierman E, Charnley M. Miniaturized pre-clinical cancer models as research and diagnostic tools. Advanced Drug Delivery Reviews.. 2014;**69-70**:52-66. DOI: 10.1016/j.addr.2013.11.010

[7] Kola I, Landis J. Can the pharmaceutical industry reduce attrition rates? Nature Reviews Drug Discovery. 2004;**3**(8):711-715. DOI: 10.1038/nrd1470

[8] Arrowsmith J, Miller P. Trial watch: Phase II and phase III attrition rates 2011-2012. Nature Reviews Drug Discovery. 2013;**12**(8):569. DOI: 10.1038/nrd4090

[9] Hay M, et al. Clinical development success rates for investigational drugs. Nature Biotechnology. 2014;**32**(1):40-51. DOI: 10.1038/nbt.2786

[10] Arrowsmith J. Trial watch: Phase II failures: 2008-2010. Nature Reviews Drug Discovery. 2011;**10**(5):328-329. DOI: 10.1038/nrd3439

[11] Venditto VJ, Szoka FC Jr. Cancer nanomedicines: So many papers and so few drugs! Advanced Drug Delivery Reviews. 2013;**65**(1):80-88. DOI: 10.1016/j.addr.2012.09.038

[12] Kamb A. What's wrong with our cancer models? Nature Reviews Drug Discovery. 2005;**4**(2):161-165. DOI: 10.1038/nrd1635

[13] Unger C, et al. Modeling human carcinomas: Physiologically relevant 3D models to improve anti-cancer drug development. Advanced Drug Delivery Reviews. 2014;**79-80**:50-67. DOI: 10.1016/j.addr.2014.10.015

[14] Cook D, et al. Lessons learned from the fate of AstraZeneca's drug pipeline: A five-dimensional framework. Nature Reviews Drug Discovery. 2014;**13**(6):419-431. DOI: 10.1038/nrd4309

[15] Pound P, et al. Where is the evidence that animal research benefits humans? BMJ. 2004;**328**(7438):514-517. DOI: 10.1136/bmj.328.7438.514

[16] Hartung T. Food for thought… on animal tests. ALTEX. 2008;**25**(1):3-16

[17] Mak IW, Evaniew N, and Ghert M. Lost in translation: Animal models and clinical trials in cancer treatment. American Journal of Translational Research. 2014;**6**(2):114-118

[18] Olson H, et al. Concordance of the toxicity of pharmaceuticals in humans and in animals. Regulatory Toxicology and Pharmacology. 2000;**32**(1):56-67. DOI: 10.1006/rtph.2000.1399

[19] van der Worp HB, et al. Can animal models of disease reliably inform human studies? PLoS Medicine. 2010;**7**(3):e1000245. DOI: 10.1371/journal.pmed.1000245

[20] Hackam DG. Translating animal research into clinical benefit. BMJ. 2007;**334**(7586):163-164. DOI: 10.1136/bmj.39104.362951.80

[21] Perel P, et al. Comparison of treatment effects between animal experiments and clinical trials: Systematic review. BMJ. 2007;**334**(7586):197. DOI: 10.1136/bmj.39048.407928.BE

[22] Gillet JP, Varma S, Gottesman MM. The clinical relevance of cancer cell lines. Journal of the National Cancer Institute. 2013;**105**(7):452-458. DOI: 10.1093/jnci/djt007

[23] Weiswald LB, Bellet D, Dangles-Marie V. Spherical cancer models in tumor biology. Neoplasia. 2015;**17**(1):1-15. DOI: 10.1016/j.neo.2014.12.004

[24] Thoma CR, et al. 3D cell culture systems modeling tumor growth determinants in cancer target discovery. Advanced Drug Delivery Reviews. 2014;**69-70**:29-41. DOI: 10.1016/j.addr.2014.03.001

[25] Yamada KM, Cukierman E. Modeling tissue morphogenesis and cancer in 3D. Cell. 2007;**130**(4):601-610. DOI: 10.1016/j.cell.2007.08.006

[26] Nath S, Devi GR. Three-dimensional culture systems in cancer research: Focus on tumor spheroid model. Pharmacology and Therapeutics. 2016;**163**:94-108. DOI: 10.1016/j.pharmthera.2016.03.013

[27] Hickman JA, et al. Three-dimensional models of cancer for pharmacology and cancer cell biology: Capturing tumor complexity in vitro/ex vivo. Biotechnology Journal. 2014;**9**(9):1115-1128. DOI: 10.1002/biot.201300492

[28] Imamura Y, et al. Comparison of 2D- and 3D-culture models as drug-testing platforms in breast cancer. Oncology Reports. 2015;**33**(4):1837-1843. DOI: 10.3892/or.2015.3767

[29] Fitzgerald KA, et al. Life in 3D is never flat: 3D models to optimise drug delivery. Journal of Controlled Release. 2015;**215**:39-54. DOI: 10.1016/j.jconrel.2015.07.020

[30] Tay CY, et al. Reality check for nanomaterial-mediated therapy with 3D biomimetic culture systems. Advanced Functional Materials. 2016;**26**(23):4046-4065. DOI: 10.1002/adfm.201600476

[31] Wenzel C, et al. 3D high-content screening for the identification of compounds that target cells in dormant tumor spheroid regions. Experimental Cell Research. 2014;**323**(1):131-143. DOI: 10.1016/j.yexcr.2014.01.017

[32] Howes AL, et al. The phosphatidylinositol 3-kinase inhibitor, PX-866, is a potent inhibitor of cancer cell motility and growth in three-dimensional cultures. Molecular Cancer Therapeutics. 2007;**6**(9):2505-2514. DOI: 10.1158/1535-7163.MCT-06-0698

[33] Roberts DL, et al. Contribution of HIF-1 and drug penetrance to oxaliplatin resistance in hypoxic colorectal cancer cells. British Journal of Cancer. 2009;**101**(8):1290-1297. DOI: 10.1038/sj.bjc.6605311

[34] Dufau I, et al. Multicellular tumor spheroid model to evaluate spatio-temporal dynamics effect of chemotherapeutics: Application to the gemcitabine/CHK1 inhibitor combination in pancreatic cancer. BMC Cancer. 2012;**12**:15. DOI: 10.1186/1471-2407-12-15

[35] Nederman T. Effects of vinblastine and 5-fluorouracil on human glioma and thyroid cancer cell monolayers and spheroids. Cancer Research. 1984;**44**(1):254-258

[36] Carlsson J, Nederman T. A method to measure the radio and chemosensitivity of human spheroids. Advances in Experimental Medicine and Biology. 1983;**159**:399-417

[37] Acker H. The use of human tumor cells grown in multicellular spheroid culture for designing and improving therapeutic strategies. Journal of Theoretical Medicine. 1998;**1**:193-207

[38] Kunz-Schughart LA, Kreutz M, Knuechel R. Multicellular spheroids: A three-dimensional in vitro culture system to study tumour biology. International Journal of Experimental Pathology. 1998;**79**(1):1-23

[39] Kobayashi H, et al. Acquired multicellular-mediated resistance to alkylating agents in cancer. Proceedings of the National Academy of Sciences of the United States of America. 1993;**90**(8):3294-3298

[40] Graham CH, et al. Rapid acquisition of multicellular drug resistance after a single exposure of mammary tumor cells to antitumor alkylating agents. Journal of the National Cancer Institute. 1994;**86**(13):975-982

[41] Kerbel RS, et al. Induction and reversal of cell adhesion-dependent multicellular drug resistance in solid breast tumors. Human Cell. 1996;**9**(4):257-264

[42] Desoize B, Jardillier J. Multicellular resistance: A paradigm for clinical resistance? Critical Reviews in Oncology/Hematology. 2000;**36**(2-3):193-207

[43] Chatzinikolaidou M. Cell spheroids: the new frontiers in in vitro models for cancer drug validation. Drug Discovery Today. 2016;**21**(9):1553-1560. DOI: 10.1016/j.drudis.2016.06.024

[44] Rodriguez-Enriquez S, et al. Energy metabolism transition in multi-cellular human tumor spheroids. Journal of Cellular Physiology. 2008;**216**(1):189-197. DOI: 10.1002/jcp.21392

[45] Fallica B, Makin G, Zaman MH. Bioengineering approaches to study multidrug resistance in tumor cells. Integrative Biology. 2011;**3**(5):529-539. DOI: 10.1039/c0ib00142b

[46] Aguirre-Ghiso JA. Models, mechanisms and clinical evidence for cancer dormancy. Nature Reviews Cancer. 2007;**7**(11):834-846. DOI: 10.1038/nrc2256

[47] Ruppender NS, et al. Dormancy in solid tumors: Implications for prostate cancer. Cancer and Metastasis Reviews. 2013;**32**(3-4):501-509. DOI: 10.1007/s10555-013-9422-z

[48] Kyle AH, Baker JH, Minchinton AI. Targeting quiescent tumor cells via oxygen and IGF-I supplementation. Cancer Research. 2012;**72**(3):801-809. DOI: 10.1158/0008-5472.CAN-11-3059

[49] Ma HL, et al. Multicellular tumor spheroids as an in vivo-like tumor model for three-dimensional imaging of chemotherapeutic and nano material cellular penetration. Molecular Imaging. 2012;**11**(6):487-498

[50] Amann A, et al. Development of an innovative 3D cell culture system to study tumour-stroma interactions in non-small cell lung cancer cells. PLoS One. 2014;**9**(3):e92511. DOI: 10.1371/journal.pone.0092511

[51] Dolznig H, et al. Organotypic spheroid cultures to study tumor-stroma interaction during cancer development. Drug Discovery Today: Disease Models. 2011;**8**(2-3):113-119. DOI: 10.1016/j.ddmod.2011.06.003

[52] Griffin JL, Shockcor JP. Metabolic profiles of cancer cells. Nature Reviews Cancer. 2004;**4**(7):551-561. DOI: 10.1038/nrc1390

[53] Landowski TH, et al. Cell adhesion-mediated drug resistance (CAM-DR) is associated with activation of NF-kappa B (RelB/p50) in myeloma cells. Oncogene. 2003;**22**(16):2417-2421. DOI: 10.1038/sj.onc.1206315

[54] Serebriiskii I, et al. Fibroblast-derived 3D matrix differentially regulates the growth and drug-responsiveness of human cancer cells. Matrix Biology. 2008;**27**(6):573-585. DOI: 10.1016/j.matbio.2008.02.008

[55] Shield K, et al. Multicellular spheroids in ovarian cancer metastases: Biology and pathology. Gynecologic Oncology. 2009;**113**(1):143-148. DOI: 10.1016/j.ygyno.2008.11.032

[56] Eke I, Cordes N. Radiobiology goes 3D: How ECM and cell morphology impact on cell survival after irradiation. Radiotherapy and Oncology. 2011;**99**(3):271-278. DOI: 10.1016/j.radonc.2011.06.007

[57] Dalton WS. The tumor microenvironment as a determinant of drug response and resistance. Drug Resistance Updates. 1999;**2**(5):285-288. DOI: 10.1054/drup.1999.0097

[58] Leong DT, Ng KW. Probing the relevance of 3D cancer models in nanomedicine research. Advanced Drug Delivery Reviews.. 2014;**79-80**:95-106. DOI: 10.1016/j.addr.2014.06.007

[59] El-Dakdouki MH, Pure E, Huang X. Development of drug loaded nanoparticles for tumor targeting. Part 2: Enhancement of tumor penetration through receptor mediated transcytosis in 3D tumor models. Nanoscale. 2013;**5**(9):3904-3911. DOI: 10.1039/c3nr90022c

[60] Hu Q, et al. F3 peptide-functionalized PEG-PLA nanoparticles co-administrated with tLyp-1 peptide for anti-glioma drug delivery. Biomaterials. 2013;**34**(4):1135-1145. DOI: 10.1016/j.biomaterials.2012.10.048

[61] Xin H, et al. Anti-glioblastoma efficacy and safety of paclitaxel-loading Angiopep-conjugated dual targeting PEG-PCL nanoparticles. Biomaterials. 2012;**33**(32):8167-8176. DOI: 10.1016/j.biomaterials.2012.07.046

[62] Jiang X, et al. Solid tumor penetration by integrin-mediated pegylated poly(trimethylene carbonate) nanoparticles loaded with paclitaxel. Biomaterials. 2013;**34**(6):1739-1746. DOI: 10.1016/j.biomaterials.2012.11.016

[63] Huang K, et al. Size-dependent localization and penetration of ultrasmall gold nanoparticles in cancer cells, multicellular spheroids, and tumors in vivo. ACS Nano. 2012;**6**(5):4483-4493. DOI: 10.1021/nn301282m

[64] Jena PV, et al. Photoluminescent carbon nanotubes interrogate the permeability of multicellular tumor spheroids. Carbon N Y. 2016;**97**:99-109. DOI: 10.1016/j.carbon.2015.08.024

[65] Yong T, et al. Domino-like intercellular delivery of undecylenic acid-conjugated porous silicon nanoparticles for deep tumor penetration. ACS Applied Materials and Interfaces. 2016;**8**(41):27611-27621. DOI: 10.1021/acsami.6b11127

[66] Oliveira MS, et al. Solid lipid nanoparticles co-loaded with doxorubicin and α-tocopherol succinate are effective against drug-resistant cancer cells in monolayer and 3-D spheroid cancer cell models. International Journal of Pharmaceutics. 2016;**512**(1):292-300. DOI: 10.1016/j.ijpharm.2016.08.049

[67] Wang X, et al. Doxorubicin delivery to 3D multicellular spheroids and tumors based on boronic acid-rich chitosan nanoparticles. Biomaterials. 2013;**34**(19):4667-4679. DOI: 10.1016/j.biomaterials.2013.03.008

[68] Wang Y, et al. Tumor-penetrating nanoparticles for enhanced anticancer activity of combined photodynamic and hypoxia-activated therapy. ACS Nano. 2017;**11**(2):2227-2238. DOI: 10.1021/acsnano.6b08731

[69] Kulkarni P, et al. Hypoxia responsive, tumor penetrating lipid nanoparticles for delivery of chemotherapeutics to pancreatic cancer cell spheroids. Bioconjugate Chemistry. 2016;**27**(8):1830-1838. DOI: 10.1021/acs.bioconjchem.6b00241

[70] Thi Thuy Duong L, et al. Evaluation of anti-HER2 scFv-conjugated PLGA–PEG nanoparticles on 3D tumor spheroids of BT474 and HCT116 cancer cells. Advances in Natural Sciences: Nanoscience and Nanotechnology. 2016;**7**(2):025004

[71] Sarisozen C, et al. Nanomedicine based curcumin and doxorubicin combination treatment of glioblastoma with scFv-targeted micelles: In vitro evaluation on 2D and 3D tumor models. European Journal of Pharmaceutics and Biopharmaceutics. 2016;**108**:54-67. DOI: 10.1016/j.ejpb.2016.08.013

[72] Yao W, et al. Folic acid-conjugated soybean protein-based nanoparticles mediate efficient antitumor ability in vitro. Journal of Biomaterials Applications. 2016;**31**(6):832-843. DOI: 10.1177/0885328216679571

[73] Jiang Y, et al. Albumin-polymer conjugate nanoparticles and their interactions with prostate cancer cells in 2D and 3D culture: Comparison between PMMA and PCL. Journal of Materials Chemistry B. 2016;**4**(11):2017-2027. DOI: 10.1039/C5TB02576A

[74] Movia D, et al. Screening the cytotoxicity of single-walled carbon nanotubes using novel 3D tissue-mimetic models. ACS Nano. 2011;**5**(11):9278-9290. DOI: 10.1021/nn203659m

[75] Lee J, et al. In vitro toxicity testing of nanoparticles in 3D cell culture. Small. 2009;**5**(10): 1213-1221. DOI: 10.1002/smll.200801788

[76] Stocke NA, et al. Toxicity evaluation of magnetic hyperthermia induced by remote actuation of magnetic nanoparticles in 3D micrometastasic tumor tissue analogs for triple negative breast cancer. Biomaterials. 2017;**120**:115-125. DOI: 10.1016/j.biomaterials.2016.12.019

[77] Dias DR, Moreira AF, Correia IJ. The effect of the shape of gold core-mesoporous silica shell nanoparticles on the cellular behavior and tumor spheroid penetration. Journal of Materials Chemistry B. 2016;**4**(47):7630-7640. DOI: 10.1039/C6TB02668K

[78] Rane TD, Armani AM. Two-photon microscopy analysis of gold nanoparticle uptake in 3D cell spheroids. PLoS One. 2016;**11**(12):e0167548. DOI: 10.1371/journal.pone.0167548

[79] Zhao J, et al. Cellular uptake and movement in 2D and 3D multicellular breast cancer models of fructose-based cylindrical micelles that is dependent on the rod length. ACS Applied Materials and Interfaces. 2016;**8**(26):16622-16630. DOI: 10.1021/acsami.6b04805

[80] Bugno J, et al. Size and surface charge of engineered poly(amidoamine) dendrimers modulate tumor accumulation and penetration: A model study using multicellular tumor spheroids. Molecular Pharmaceutics. 2016;**13**(7):2155-2163. DOI: 10.1021/acs.molpharmaceut.5b00946

[81] Arranja A, et al. Interactions of Pluronic nanocarriers with 2D and 3D cell cultures: Effects of PEO block length and aggregation state. Journal of Controlled Release. 2016;**224**:126-135. DOI: 10.1016/j.jconrel.2016.01.014

[82] Li HJ, et al. Stimuli-responsive clustered nanoparticles for improved tumor penetration and therapeutic efficacy. Proceedings of the National Academy of Sciences of the United States of America. 2016;**113**(15):4164-4169. DOI: 10.1073/pnas.1522080113

[83] Corvaglia S, Guarnieri D, and Pompa PP. Boosting the therapeutic efficiency of nanovectors: Exocytosis engineering. Nanoscale. 2017;**9**(11):3757-3765. DOI: 10.1039/C7NR00364A

[84] Russell WMS, Burch RL. The Principles of Humane Experimental Technique. London, UK: Methuen & Co, Ltd; 1959

[85] Vinci M, et al. Advances in establishment and analysis of three-dimensional tumor spheroid-based functional assays for target validation and drug evaluation. BMC Biology. 2012;**10**:29. DOI: 10.1186/1741-7007-10-29

[86] Nyga A, Cheema U, Loizidou M. 3D tumour models: Novel in vitro approaches to cancer studies. Journal of Cell Communication and Signaling. 2011;**5**(3):239-248. DOI: 10.1007/s12079-011-0132-4

[87] Scannell JW, et al. Diagnosing the decline in pharmaceutical R&D efficiency. Nature Reviews Drug Discovery. 2012;**11**(3):191-200. DOI: 10.1038/nrd3681

[88] Mehta G, et al. Opportunities and challenges for use of tumor spheroids as models to test drug delivery and efficacy. Journal of Controlled Release. 2012;**164**(2):192-204. DOI: 10.1016/j.jconrel.2012.04.045

[89] Subramanian J, et al. Review of ongoing clinical trials in non-small-cell lung cancer: A status report for 2012 from the ClinicalTrials.gov Web site. Journal of Thoracic Oncology. 2013;**8**(7):860-865. DOI: 10.1097/JTO.0b013e318287c562

[90] Subramanian J, et al. Review of ongoing clinical trials in non-small cell lung cancer: A status report for 2009 from the ClinicalTrials.gov website. Journal of Thoracic Oncology. 2010;**5**(8):1116-1119. DOI: 10.1097/JTO.0b013e3181e76159

[91] Davies A. Cell Suspension Medium and Cell Suspension Medium Additive for the Three Dimensional Growth of Cells. 2013, Google Patents

[92] Zanoni M, et al. 3D tumor spheroid models for in vitro therapeutic screening: A systematic approach to enhance the biological relevance of data obtained. Scientific Reports. 2016;**6**:19103. DOI: 10.1038/srep19103

[93] Zschenker O, et al. Genome-wide gene expression analysis in cancer cells reveals 3D growth to affect ECM and processes associated with cell adhesion but not DNA repair. PLoS One. 2012;**7**(4):e34279. DOI: 10.1371/journal.pone.0034279

[94] Hirschhaeuser F, et al. Multicellular tumor spheroids: An underestimated tool is catching up again. Journal of Biotechnology. 2010;**148**(1):3-15. DOI: 10.1016/j.jbiotec.2010.01.012

[95] Costa EC, et al. 3D tumor spheroids: An overview on the tools and techniques used for their analysis. Biotechnology Advances. 2016;**34**(8):1427-1441. DOI: 10.1016/j.biotechadv.2016.11.002

[96] Rehfeldt F, et al. Cell responses to the mechanochemical microenvironment—Implications for regenerative medicine and drug delivery. Advanced Drug Delivery Reviews. 2007;**59**(13):1329-1339. DOI: 10.1016/j.addr.2007.08.007

[97] Elliott NT, Yuan F. A review of three-dimensional in vitro tissue models for drug discovery and transport studies. Journal of Pharmaceutical Sciences. 2011;**100**(1):59-74. DOI: 10.1002/jps.22257

[98] Liang Y, et al. A cell-instructive hydrogel to regulate malignancy of 3D tumor spheroids with matrix rigidity. Biomaterials. 2011;**32**(35):9308-9315. DOI: 10.1016/j.biomaterials.2011.08.045

[99] Shintani Y, et al. Collagen I promotes epithelial-to-mesenchymal transition in lung cancer cells via transforming growth factor-beta signaling. American Journal of Respiratory Cell and Molecular Biology. 2008;**38**(1):95-104. DOI: 10.1165/rcmb.2007-0071OC

[100] Kalluri R., Weinberg RA. The basics of epithelial-mesenchymal transition. Journal of Clinical Investigation. 2009;**119**(6):1420-1428. DOI: 10.1172/JCI39104

[101] Lamouille S, Xu J, Derynck R. Molecular mechanisms of epithelial-mesenchymal transition. Nature Reviews Molecular Cell Biology. 2014;**15**(3):178-196. DOI: 10.1038/nrm3758

[102] Richardson F, et al. The evaluation of E-Cadherin and vimentin as biomarkers of clinical outcomes among patients with non-small cell lung cancer treated with erlotinib as second- or third-line therapy. Anticancer Research. 2012;**32**(2):537-552

[103] Oliveira R, et al. Contribution of gap junctional communication between tumor cells and astroglia to the invasion of the brain parenchyma by human glioblastomas. BMC Cell Biology. 2005;**6**(1):7. DOI: 10.1186/1471-2121-6-7

[104] Osanai M, et al. Epigenetic silencing of occludin promotes tumorigenic and metastatic properties of cancer cells via modulations of unique sets of apoptosis-associated genes. Cancer Research. 2006;**66**(18):9125-9133. DOI: 10.1158/0008-5472.CAN-06-1864

[105] Jinn Y, Inase N. Connexin 43, E-cadherin, beta-catenin and ZO-1 expression, and aberrant methylation of the connexin 43 gene in NSCLC. Anticancer Research. 2010;**30**(6): 2271-2278

[106] Hazrin-Chong NH, Manefield M. An alternative SEM drying method using hexamethyldisilazane (HMDS) for microbial cell attachment studies on sub-bituminous coal. Journal of Microbiological Methods. 2012;**90**(2):96-99. DOI: 10.1016/j.mimet.2012.04.014

[107] Braet F, De Zanger R, Wisse E. Drying cells for SEM, AFM and TEM by hexamethyldisilazane: A study on hepatic endothelial cells. Journal of Microscopy. 1997;**186**(Pt 1):84-87

[108] Bell DC. Contrast mechanisms and image formation in helium ion microscopy. Microscopy and Microanalysis. 2009;**15**(2):147-153. DOI: 10.1017/S1431927609090138

[109] Bazou D, et al. Elucidation of flow-mediated tumour cell-induced platelet aggregation using an ultrasound standing wave trap. British Journal of Pharmacology. 2011;**162**(7):1577-1589. DOI: 10.1111/j.1476-5381.2010.01182.x

[110] Rice WL, et al. High resolution helium ion scanning microscopy of the rat kidney. PLoS One. 2013;**8**(3):e57051. DOI: 10.1371/journal.pone.0057051

[111] Bazou D, et al. Imaging of human colon cancer cells using He-Ion scanning microscopy. Journal of Microscopy. 2011;**242**(3):290-294. DOI: 10.1111/j.1365-2818.2010.03467.x

[112] Mohamed BM, et al. Citrullination of proteins: A common post-translational modification pathway induced by different nanoparticles in vitro and in vivo. Nanomedicine (London, England). 2012;**7**(8):1181-1195. DOI: 10.2217/nnm.11.177

[113] Bauer H, et al. The dual role of zonula occludens (ZO) proteins. Journal of Biomedicine & Biotechnology. 2010;**2010**:402593. DOI: 10.1155/2010/402593

[114] Friedrich J, et al. Spheroid-based drug screen: Considerations and practical approach. Nature Protocols. 2009;**4**(3):309-324. DOI: 10.1038/nprot.2008.226

[115] Ju RJ, Mu LM, Lu WL. Targeting drug delivery systems for circumventing multidrug resistance of cancers. Therapeutic Delivery. 2013;**4**(6):667-671. DOI: 10.4155/tde.13.39

[116] Kim H, Phung Y, Ho M. Changes in global gene expression associated with 3D structure of tumors: An ex vivo matrix-free mesothelioma spheroid model. PLoS One. 2012;**7**(6):e39556. DOI: 10.1371/journal.pone.0039556

[117] Movia D, et al. A safe-by-design approach to the development of gold nanoboxes as carriers for internalization into cancer cells. Biomaterials. 2014;**35**(9):2543-2557. DOI: 10.1016/j.biomaterials.2013.12.057

[118] Ivascu A, Kubbies M. Rapid generation of single-tumor spheroids for high-throughput cell function and toxicity analysis. Journal of Biomolecular Screening. 2006;**11**(8):922-932. DOI: 10.1177/1087057106292763

[119] Del Duca D, Werbowetski T, Del Maestro RF. Spheroid preparation from hanging drops: Characterization of a model of brain tumor invasion. Journal of Neuro-Oncology. 2004;**67**(3):295-303

[120] Neto AI, et al. A novel hanging spherical drop system for the generation of cellular spheroids and high throughput combinatorial drug screening. Biomaterials Science. 2015;**3**(4):581-585. DOI: 10.1039/c4bm00411f

[121] Ivascu A, Kubbies M. Diversity of cell-mediated adhesions in breast cancer spheroids. International Journal of Oncology. 2007;**31**(6):1403-1413

[122] Xiang X, et al. The development and characterization of a human mesothelioma in vitro 3D model to investigate immunotoxin therapy. PLoS One. 2011;**6**(1):e14640. DOI: 10.1371/journal.pone.0014640

[123] Wright MH, et al. Brca1 breast tumors contain distinct CD44+/CD24- and CD133+ cells with cancer stem cell characteristics. Breast Cancer Research. 2008;**10**(1):R10. DOI: 10.1186/bcr1855

[124] Takaishi S, et al. Identification of gastric cancer stem cells using the cell surface marker CD44. Stem Cells. 2009;**27**(5):1006-1020. DOI: 10.1002/stem.30

[125] Cheng V, et al. High-content analysis of tumour cell invasion in three-dimensional spheroid assays. Oncoscience. 2015;**2**(6):596-606. DOI: 10.18632/oncoscience.171

[126] Matsuda Y, et al. Morphological and cytoskeletal changes of pancreatic cancer cells in three-dimensional spheroidal culture. Medical Molecular Morphology. 2010;**43**(4):211-217. DOI: 10.1007/s00795-010-0497-0

[127] Hardelauf H, et al. Microarrays for the scalable production of metabolically relevant tumour spheroids: A tool for modulating chemosensitivity traits. Lab on a Chip. 2011;**11**(3):419-428. DOI: 10.1039/c0lc00089b

[128] Fischbach C, et al. Engineering tumors with 3D scaffolds. Nature Methods. 2007;**4**(10):855-860. DOI: 10.1038/nmeth1085

[129] Wartenberg M, et al. Tumor-induced angiogenesis studied in confrontation cultures of multicellular tumor spheroids and embryoid bodies grown from pluripotent embryonic stem cells. FASEB Journal. 2001;**15**(6):995-1005

[130] Unsworth BR, Lelkes PI. Growing tissues in microgravity. Nature Medicine. 1998;**4**(8): 901-907

[131] Mazzoleni G, Di Lorenzo D, Steimberg N. Modelling tissues in 3D: The next future of pharmaco-toxicology and food research? Genes & Nutrition. 2009;**4**(1):13-22. DOI: 10.1007/s12263-008-0107-0

[132] Thoma CR, et al. A high-throughput-compatible 3D microtissue co-culture system for phenotypic RNAi screening applications. Journal of Biomolecular Screening. 2013;**18**(10):1330-1337. DOI: 10.1177/1087057113499071

[133] HTStec. 3D Cell Culture Trends 2011. 2011. Available at: http://www.htstec.com/consultancyitem.aspx?Item=374

[134] Graf BW, Boppart SA. Imaging and analysis of three-dimensional cell culture models. Methods in Molecular Biology. 2010;**591**:211-227. DOI: 10.1007/978-1-60761-404-3_13

[135] http://www.perkinelmer.com/pdfs/downloads/APP_Opera-Microtissue-Cores.pdf [Accessed on: March 2017]

[136] Hama H, et al. Scale: A chemical approach for fluorescence imaging and reconstruction of transparent mouse brain. Nature Neuroscience. 2011;**14**(11):1481-1488. DOI: 10.1038/nn.2928

[137] Zhang JZ, et al. The use of spectroscopic imaging and mapping techniques in the characterisation and study of DLD-1 cell spheroid tumour models. Integrative Biology (Camb). 2012;**4**(9):1072-1080. DOI: 10.1039/c2ib20121f

[138] https://3dbiomatrix.com/wp-content/uploads/2013/10/Perfecta3D-HDP1096-Protocols_SF_Spheroid-Formation_05_13.pdf [Accessed on: January 2017]

[139] https://3dbiomatrix.com/wp-content/uploads/2013/10/Perfecta3D-HDP1096-Protocols_SF_Exchange_12-15-12.pdf [Accessed on: January 2017]

[140] https://3dbiomatrix.com/wp-content/uploads/2014/02/Perfecta3D-Protocols_SF_Transfer-96well-2_2014.pdf [Accessed on: January 2017]

[141] Rothen-Rutishauser B, et al. In vitro models of the human epithelial airway barrier to study the toxic potential of particulate matter. Expert Opinion on Drug Metabolism & Toxicology. 2008;**4**(8):1075-1089. DOI: 10.1517/17425255.4.8.1075

[142] Caino MC, et al. Non-small cell lung carcinoma cell motility, rac activation and metastatic dissemination are mediated by protein kinase C epsilon. PLoS One. 2012;**7**(2):e31714. DOI: 10.1371/journal.pone.0031714

[143] Gazdar AF, et al. Lung cancer cell lines as tools for biomedical discovery and research. Journal of the National Cancer Institute. 2010;**102**(17):1310-1321. DOI: 10.1093/jnci/djq279

[144] Mohamed BM, et al. Citrullination as early-stage indicator of cell response to single-walled carbon nanotubes. Scientific Reports. 2013;**3**:1124. DOI: 10.1038/srep01124

[145] Mohamed BM, et al. Activation of stress-related signalling pathway in human cells upon SiO_2 nanoparticles exposure as an early indicator of cytotoxicity. Journal of Nanobiotechnology. 2011;**9**:29. DOI: 10.1186/1477-3155-9-29

[146] Verma NK, et al. Autophagy induction by silver nanowires: A new aspect in the biocompatibility assessment of nanocomposite thin films. Toxicology and Applied Pharmacology. 2012;**264**(3):451-461. DOI: 10.1016/j.taap.2012.08.023

[147] Verma NK, et al. Magnetic core-shell nanoparticles for drug delivery by nebulization. J Nanobiotechnology. 2013;**11**:1. DOI: 10.1186/1477-3155-11-1

[148] Singh M, et al. Silver nanowires as prospective carriers for drug delivery in cancer treatment: An in vitro biocompatibility study on lung adenocarcinoma cells and fibroblasts. European Journal of Nanomedicine. 2013;**5**(4):195-204. DOI: 10.1515/ejnm-2013-0024

[149] Stratmann AT, et al. Establishment of a human 3D lung cancer model based on a biological tissue matrix combined with a Boolean in silico model. Molecular Oncology. 2014;**8**(2):351-365. DOI: 10.1016/j.molonc.2013.11.009

[150] Godugu C, et al. AlgiMatrix based 3D cell culture system as an in-vitro tumor model for anticancer studies. PLoS One. 2013;**8**(1):e53708. DOI: 10.1371/journal.pone.0053708

[151] Cichon MA, et al. Growth of lung cancer cells in three-dimensional microenvironments reveals key features of tumor malignancy. Integrative Biology (Camb). 2012;**4**(4):440-448. DOI: 10.1039/c1ib00090j

[152] Xu F, et al. A three-dimensional in vitro ovarian cancer coculture model using a high-throughput cell patterning platform. Biotechnology Journal. 2011;**6**(2):204-212. DOI: 10.1002/biot.201000340

[153] Friedrich J, Ebner R, Kunz-Schughart LA. Experimental anti-tumor therapy in 3-D: Spheroids--old hat or new challenge? International Journal of Radiation Biology. 2007;**83**(11-12):849-871. DOI: 10.1080/09553000701727531

[154] Nakamura K, et al. Apoptosis induction of human lung cancer cell line in multicellular heterospheroids with humanized antiganglioside GM2 monoclonal antibody. Cancer Research. 1999;**59**(20):5323-5330

[155] Krueger S, et al. Interactions between human colon carcinoma cells, fibroblasts and monocytic cells in coculture—Regulation of cathepsin B expression and invasiveness. Cancer Letters. 2005;**223**(2):313-322. DOI: 10.1016/j.canlet.2004.09.050

[156] Paduch R and Niedziela P. TGF-beta1 influence on TNF-alpha production and sTNF-Rs shedding in a coculture of colon carcinoma cell spheroids with normal cells. In Vitro Cellular and Developmental Biology—Animal. 2009;**45**(7):371-377. DOI: 10.1007/s11626-009-9190-9

[157] Brouty-Boye D, et al. Fibroblast-mediated differentiation in human breast carcinoma cells (MCF-7) grown as nodules in vitro. International Journal of Cancer. 1994;**56**(5):731-735

[158] Seidl P, et al. Three-dimensional fibroblast-tumor cell interaction causes downregulation of RACK1 mRNA expression in breast cancer cells in vitro. International Journal of Cancer. 2002;**102**(2):129-136. DOI: 10.1002/ijc.10675

[159] Schuster U, et al. A heterologous in vitro coculture system to study interaction between human bladder cancer cells and fibroblasts. Journal of Urology. 1994;**151**(6):1707-1711

[160] Kunz-Schughart LA, et al. A heterologous 3-D coculture model of breast tumor cells and fibroblasts to study tumor-associated fibroblast differentiation. Experimental Cell Research. 2001;**266**(1):74-86. DOI: 10.1006/excr.2001.5210

[161] Kim SH, et al. Human lung cancer-associated fibroblasts enhance motility of non-small cell lung cancer cells in co-culture. Anticancer Research. 2013;**33**(5):2001-2009

[162] An J, et al. Significance of cancer-associated fibroblasts in the regulation of gene expression in the leading cells of invasive lung cancer. Journal of Cancer Research and Clinical Oncology. 2013;**139**(3):379-388. DOI: 10.1007/s00432-012-1328-6

[163] Walzl A, et al. The resazurin reduction assay can distinguish cytotoxic from cytostatic compounds in spheroid screening assays. Journal of Biomolecular Screening. 2014;**19**(7):1047-1059. DOI: 10.1177/1087057114532352

[164] Ng KW, Leong DT, Hutmacher DW. The challenge to measure cell proliferation in two and three dimensions. Tissue Engineering. 2005;**11**(1-2):182-191. DOI: 10.1089/ten.2005.11.182

[165] Movia D, Giordani S. Toxicity of carbon nanotubes. In: Handbook of Green Chemistry. Wiley-VCH Verlag GmbH & Co. KGaA; Weinheim, Germany. 2010. DOI: 10.1002/9783527628698.hgc091

[166] Cho EC, Zhang Q, Xia Y. The effect of sedimentation and diffusion on cellular uptake of gold nanoparticles. Nature Nanotechnology. 2011;**6**(6):385-391. DOI: 10.1038/nnano.2011.58

IntechOpen